

**FINITE ELEMENT ANALYSIS OF
ADVANCED COMPOSITE SANDWICH PANEL
CORE GEOMETRIES FOR BLAST MITIGATION**

by

Nathan P. Mayercsik

A thesis submitted to the Faculty of the University of Delaware in partial fulfillment
of the requirements for the degree of Honors Bachelor of Civil Engineering with
Distinction.

Spring 2010

Copyright 2010 Nathan P. Mayercsik
All Rights Reserved

**FINITE ELEMENT ANALYSIS OF
ADVANCED COMPOSITE SANDWICH PANEL
CORE GEOMETRIES FOR BLAST MITIGATION**

by

Nathan P. Mayercsik

Approved: _____
Jennifer Righman McConnell, Ph.D.
Professor in charge of thesis on behalf of the Advisory Committee

Approved: _____
Allen A. Jayne, Ph.D.
Committee member from the Department of Civil & Environmental
Engineering

Approved: _____
James Glancey, Ph.D.
Committee member from the Board of Senior Thesis Readers

Approved: _____
Alan Fox, Ph.D.
Director, University Honors Program

ACKNOWLEDGMENTS

I must first acknowledge Dr. Jennifer Righman McConnell for remembering my interest in performing undergraduate research and subsequently inviting me into her office to discuss this exciting prospect. Without her tireless guidance, my efforts would be in vain. I must also thank the United States Department of Defense for funding this work and for its continued efforts to keep America free and safe. My work here is also deeply indebted to Dennis Helmstetter and Su Hong for their hours of labor on this project.

TABLE OF CONTENTS

LIST OF TABLES	vi
LIST OF FIGURES	vii
ABSTRACT	ix

Chapter

1	INTRODUCTION	1
	1.1 Motivation for Research	1
	1.2 Scope of Research	2
	1.3 Thesis Organization.....	2
2	LITERATURE REVIEW	4
	2.1 Introduction	4
	2.2 Helmstetter’s Research.....	4
	2.3 Other FEM Work.....	7
	2.3.1 LS-Dyna Analysis of Polyurethane and Polyurea Interlayers	7
	2.3.2 Analytical Modeling Comparison to ABAQUS Results	10
	2.4 Work Post-Helmstetter	11
	2.5 Conclusions	11
3	MODELING BLASTS	13
	3.1 Introduction	13
	3.2 Blast Effects.....	13
	3.2.1 Pressure-versus-Time Relationships	14
	3.2.2 Pressure-versus-Time Equations	17
	3.3 MATLAB Modeling.....	19

4	CONSTRUCTING FINITE ELEMENT MODELS	25
4.1	Introduction	25
4.2	Model Generation	25
4.2.1	Drawing and Mapping	25
4.2.2	Imperfection Files	27
4.3	Helmstetter's FEM	28
4.4	Selected Analysis File	31
5	PARAMETRIC STUDY	32
5.1	Introduction	32
5.2	Parameters	32
5.3	Loading	34
5.4	Results	35
5.4.1	Deformed Shape	35
5.4.2	Total Loads at Stiffener Bases	36
5.4.3	Maximum Moment	37
5.4.4	Total Reaction	39
5.4.5	Total Reaction Normalized by Total Blast Overpressure	41
5.4.6	Total Reaction Normalized by Core Volume	43
5.5	Evaluation of Metrics	44
5.6	Data Analysis	46
5.7	Error Analysis	49
5.8	Conclusion	50
6	CONCLUSIONS	52
6.1	Summary of Work	52
6.2	Conclusions	53
6.3	Future Work	54
	WORKS CITED	56
	APPENDIX A: MATLAB FILES	57
	APPENDIX B: ERROR ANALYSIS	68
	APPENDIX C: FINITE ELEMENT CODES	69

LIST OF TABLES

Table 2.1:	Number of Stiffeners Failed versus Panel Strength (w/EV_{core}), from Helmstetter 2009	7
Table 4.1:	Material properties for FEM input file	27
Table 4.2:	Deflections for alternative modeling strategies	30
Table 5.1:	Web spacings, heights, and S_w/H ratios investigated	33
Table 5.2:	Equivalent TNT masses associated with Helmstetter's 94 J experiment	34
Table 5.3:	Time step of initial frame	36
Table 5.4:	Stress values from ABAQUS probe for a sample element.....	37
Table 5.5:	Magnitudes of Overpressure for Each Model	41
Table 5.6:	Core Volumes	44
Table 5.7:	Summary of Metrics Used to Assess Optimum Design	45
Table 5.8:	Model numbers and corresponding S_w/H ratios.....	45
Table 5.9:	Theoretical Moments, Probed Moment, and Percent Difference	49

LIST OF FIGURES

Figure 2.1:	Web Configurations Analyzed by Helmstetter: (a) Straight Stiffener Design (b) Angled Stiffener Design, and (c) Combination Stiffener Design.....	5
Figure 2.2:	Beam on an Elastic Foundation (Boresi et al 2003).....	5
Figure 2.3:	Finite element solution domain and mesh (Bahei-El-Din & Dvorak 2007).....	9
Figure 2.4:	Midspan deflection at outer and inner surface (Bahei-El-Din & Dvorak 2007).....	10
Figure 2.5:	Variation of critical impulse of failure with varying core material properties (Hoo-Fatt and Palla 2009).....	11
Figure 3.1:	Pressure versus time profile: (a) theoretical curve and (b) distribution assumed herein.....	16
Figure 3.2:	Generation of blast load on surface.....	20
Figure 3.3:	Parameters Needed to Write ABAQUS Load Input.....	21
Figure 3.4:	Schematic of MATLAB files used to generate outputs from inputs	23
Figure 5.1:	Sum of stresses in bottom elements at stiffener bases.	37
Figure 5.2:	Moment along bottom facesheet due to stiffener loads.....	38
Figure 5.3:	Maximum moment at bottom facesheet.....	39
Figure 5.4	Method of obtaining a distributed load	40
Figure 5.5:	Approximate magnitude of reaction stress at bottom facesheet necessary for static equilibrium.....	40

Figure 5.6: Percent reduction in peak overpressure.....	42
Figure 5.7: Overpressure Reduction Factor, Given by Reaction/Overpressure.....	43
Figure 5.8: Reaction Normalized by Core Volume	44
Figure 5.9: Surface Created by Equation 5.7.....	48
Figure 5.10: Surface Created by Equation 5.7 (Detail to Show Moments)	48
Figure 5.11: Correlation of Theoretical Moment to Probed Moment.....	50

ABSTRACT

The ever-present threat of terrorist activity – made plain by devastating events in the late twentieth and early twenty-first centuries – warrants detailed investigation into ever smarter materials and methods of combating the terrorist offense with a well-engineered defense. While the literature on the subject is voluminous, the complexity of the problem justifies continued research. This thesis in particular represents a continuation of previous experimental, analytical, and finite element modeling at the University of Delaware. With a panel typology utilizing horizontal facesheets separated by a core comprised of rows of stiffeners perpendicular to the facesheets established as optimal in previous papers, this research seeks to both perfect the previous finite element model and use it to glean some optimized geometric parameters.

MATLAB code provided a more accurate load profile for a chemical explosion based on Kinney and Graham's work. Analyses of varying connection and imperfection inputs in ABAQUS files honed the previous finite element files to more accurately model experimental results. Using the results, a parametric study of core geometries was executed to observe the effects of various core geometries. The analyses suggest that the ratio of stiffener spacing-to-height is a governing factor in decreasing the force effect on a protected structure.

Chapter 1

INTRODUCTION

1.1 Motivation for Research

In his famous “Four Freedoms” speech, President Roosevelt famously ranked freedom from fear alongside freedom of speech, of religion, and from want – liberties American have always held dear. In the twenty-first century, freedom from fear manifests itself as a freedom from the ever-uncertain threat of terrorist attack. Military vehicles and structures are in need of defensive shielding against explosives. This warrants research into innovative structures made from better materials which can sustain impulse loading. The burden falls on civil engineers to protect the environment that they have built.

Composite sandwich structures show great promise to this end, both in their strength and ability to absorb the energy generated by blast loadings. While protective structures date to the Second World War and garnered more research interest during the Cold War, their reliance on reinforced concrete rendered researchers without a material with a high strength-to-weight ratio. Advanced composites can be crafted into any shape, and the scope of possible configurations to alter material properties seems limitless. With the scope of possibilities so vast, and the analyses so complex, engineers would benefit greatly from understanding the effect of simple geometric parameters, and a simple empirical equation incorporating these effects could greatly streamline panel design.

1.2 Scope of Research

All research herein is a continuation of the funded project “Mitigation of Blast Forces Through Advanced Composite Materials,” funded by the Department of Defense with Dr. Jennifer McConnell as Principal Investigator. In particular, this particular thesis seeks to utilize, perfect, and extend work reported in “Analysis Procedure for Optimizing the Core of Composite Sandwich Panels for Blast Resistance,” by Dennis Helmstetter (2009). The experimental testing used for model verification, the rationale for perpendicular core stiffeners, and the preliminary use of ABAQUS for finite element analysis all lie within Helmstetter’s research.

Helmstetter (2009) suggested conducting a parametric study of different core geometries and suggested developing a method of applying alternative load profiles that simulate a blast load profile. This was born of the assumption that his model was a reasonably valid simulation of a lab experiment. Therefore, the scope of this project has three main components: correcting past errors and refining previous finite element models, developing an efficient means for imputing a realistic blast profile into the finite element model, and using the refined finite element model to study the effect of changing the geometric parameters of the core on the panels’ blast mitigation performance.

1.3 Thesis Organization

Naturally, this work opens with a review of literature. As the topic is vast, the literature review has been truncated to analyzing Helmstetter’s thesis and publications post-Helmstetter’s thesis, along with a review of some literature regarding finite element analysis of composite sandwich panels used for blast mitigation produced in the past few years. Additional information regarding the

precursor to this work may be found in Section 2.2. The following chapters of this work chart the progress of the project. Chapter 3 discusses blast loading and maps out the design of MATLAB code to generate script which can be analyzed by ABAQUS as a series of time-varying concentrated loads using the *CLOAD command. Chapter 4 provides information about constructing the models. Therein the reader will find improvements that helped Helmstetter's files deflect more accurately. Finally, Chapter 5 presents the results of the parametric study. Chapter 5 also presents several metrics by which the models may be judged in an attempt to arrive at an optimum solution. Chapter 6 concludes the work, with an overview of the thesis and suggestions for further work.

Appendix A provides the MATLAB codes discussed in Chapter 3.

Appendix B is an error analysis for some of the data manipulations performed in Chapter 5. Appendix C contains an example of a mode shape file and analysis file as explained in Chapter 4.

Chapter 2

LITERATURE REVIEW

2.1 Introduction

As the scope of this work serves as a continuation of the work done by Helmstetter (2009), the natural frame of reference for a review of literature will be Helmstetter's own work. The review then explores select publications regarding blast mitigation through composite sandwich structures post-2009.

2.2 Helmstetter's Research

Helmstetter investigated composite laminates, stitched composites, fiber-metal laminates, and sandwich panels, and concluded that sandwich panels "...offer high stiffness in both flexural and in-plane directions, while maintaining a lightweight frame," thereby focusing the remainder of his research on sandwich panels. He assessed three web configurations in Chapter 4 of his work: straight stiffener design, angled stiffener design, and combination design (Figure 2.1).

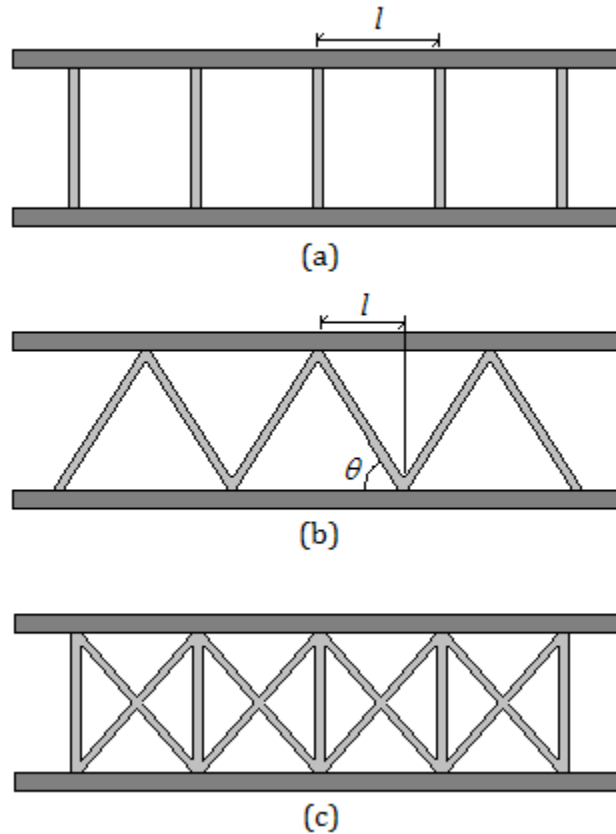


Figure 2.1: Web Configurations Analyzed by Helmstetter: (a) Straight Stiffener Design (b) Angled Stiffener Design, and (c) Combination Stiffener Design

The panels were analyzed as a beam on an elastic foundation which is described in Boresi et al (2003), and shown in Figure 2.2.

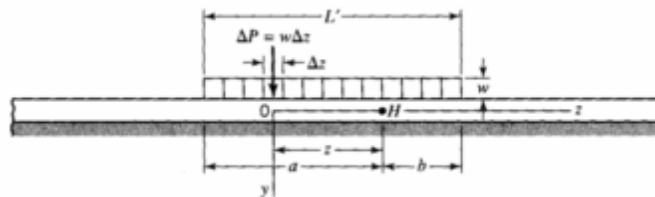


Figure 2.2: Beam on an Elastic Foundation (Boresi et al 2003).

An optimum panel configuration was chosen using analytical methods via the following equations found in Boresi et al (2003):

$$y_H = \frac{w}{2k}(2 - D_{\beta a} - D_{\beta b}) \quad (2.1)$$

Where y_H is the deflection at any point along a beam on an elastic foundation, w is the load per unit length and $D_{\beta a}$, $D_{\beta b}$, and k are given by

$$D_{\beta z} = e^{-\beta z} \cos \beta z \quad (2.2)$$

$$D_{\beta z} = e^{-\beta z} \cos \beta z \quad (2.3)$$

$$k = \frac{K}{l} \quad (2.4)$$

where K is the spring constant (i.e. axial stiffness of the stiffeners), l is the stiffener spacing, E is the modulus of elasticity of the facesheet, and I_x is the moment of inertia of the facesheet. As shown in Figure 2.2, a and b represent the boundaries of the loading profile, while z is the independent variable along the beam. Further derivations for the load causing failure can be found in the remainder of Chapter 4 of Helmstetter's work. The strengths of panels with stiffener geometries shown in Figure 2.1 were normalized by E to give strength irrespective of material properties. In order to assess efficiency of the panel apart from strength, the results were further normalized by the core volumes (V_{core}). These normalized values are found in Table 2.1 (where the results are presented in w/EV_{core}). The higher strengths afforded by the straight stiffener design justifies devoting further research into this particular panel configuration's performance under blast loads. For this reason, Helmstetter chose to

create finite element models of straight stiffener composite panels. Helmstetter’s finite element analysis is discussed in Chapter 4.

Table 2.1: Number of Stiffeners Failed versus Panel Strength (w/EV_{core}), from Helmstetter 2009

Number of Failed Stiffeners	Straight Design	Angled Design	Combination Design
1	5.598E-05	2.827E-05	2.276E-05
3	5.624E-05	2.832E-05	2.294E-05
5	5.686E-05	2.847E-05	2.335E-05
7	5.804E-05	2.887E-05	2.399E-05
9	6.009E-05	2.970E-05	2.501E-05
11	6.341E-05	3.123E-05	2.644E-05
13	6.840E-05	3.372E-05	2.844E-05

2.3 Other FEM Work

A review of literature contemporary to Helmstetter’s research suggests that other investigations on the topic of blast mitigation through advanced composites remain focused on foam-core composites without web stiffeners. Sections 2.3.1 and 2.3.2 discuss other finite element analysis work in LS-Dyna and ABAQUS, respectively.

2.3.1 LS-Dyna Analysis of Polyurethane and Polyurea Interlayers

Bahei-El-Din and Dvorak published an analysis of composite sandwich panels for blast loading in Journal of Sandwich Structures and Materials in 2007. Their work used LS-Dyna to evaluate the value of adding polyurethane (PUR) and

polyurea interlayers between the facesheets and foam cores of sandwich panels. The control analysis, termed "Design 1," had no such interlayers, while "Design 2A" contained a polyurethane interlayer and "Design 2B" contained a polyurea interlayer.

Using brick elements, the authors input the schematic shown in Figure 2.3 into LS-Dyna for the finite element models. All designs used elements with lengths equal to 1.0 mm in the X_2 direction. All designs used elements that were 5.0 mm in the X_1 direction. Design 1 used an element size of 5.0 mm for H100 foam in the X_3 direction, while Designs 2A and 2B used elements that were 4.5 mm in the X_3 direction (this ensures a ten-element thickness for the H100 foam for all three models). The interlayers in Designs 2A and 2B were divided into 10 elements spanning a total of 5.0 mm in the X_3 direction (Figure 2.3). The facesheets were assumed linearly elastic during loading and were modeled as homogeneous orthotropic materials using LS-Dyna Material Type 2, while the foam cores were modeled using Material Type 63. The polyurethane interlayer and polyurea interlayer used LS-DYNA Material Types 7 and 10, respectively. The loading assumed a peak overpressure of 100 MPa.

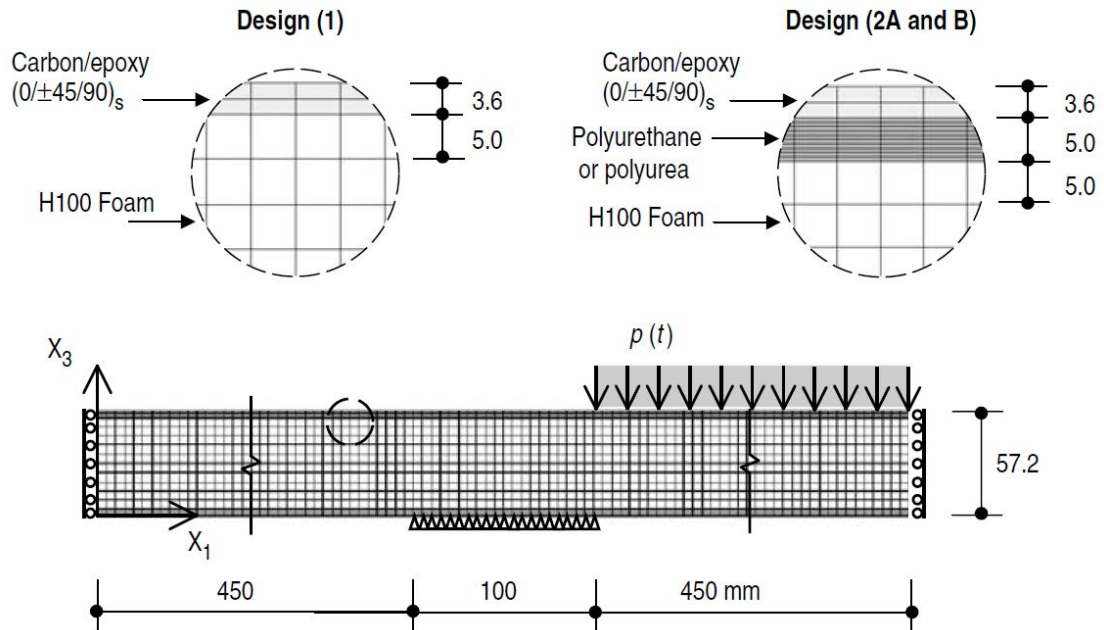


Figure 2.3: Finite element solution domain and mesh (Bahei-El-Din & Dvorak 2007)

The authors concluded that the interlayers provided "significant protection" to the foam core and reduced kinetic energy imparted by impulse. Figure 2.4 shows midspan deflection at the outer and inner surfaces (akin to the top and bottom facesheets, as they are referred to by Helmstetter and in the rest of this work), thereby demonstrating the advantage of the interlayers in mitigating deflection. Overall, the addition of the interlayers dissipated energy and reduced deflections and facesheet strains.

While this work does not explore foam core composites, the modeling techniques serve as a comparison. Both Helmstetter and Bahei-El-Din & Dvorak used orthotropic facesheets.

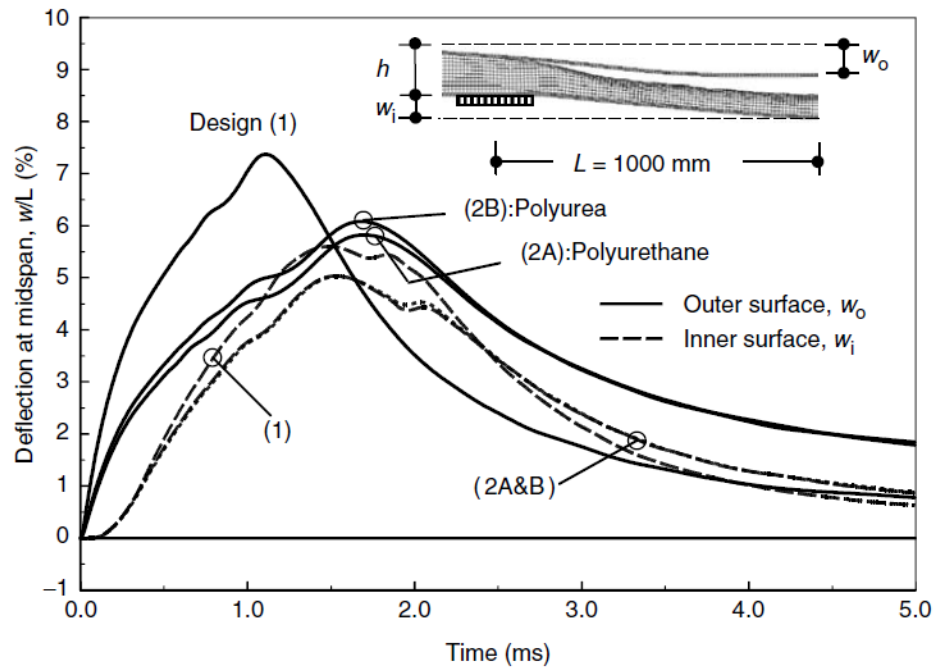


Figure 2.4: Midspan deflection at outer and inner surface (Bahei-El-Din & Dvorak 2007)

2.3.2 Analytical Modeling Comparison to ABAQUS Results

Hoo-Fatt and Palla's work (2009) sought to develop analytical equations which would match finite element results. The focus was therefore primarily based on theory rather than finite element inputs, with ABAQUS models serving as the means for comparison. The panels observed were E-glass vinyl ester facesheets separated by either H100 or H200 PVC foam cores. Hoo-Fatt and Palla's work used four-node, reduced integration shell elements (ABAQUS element type S4R) for the facesheets and continuum 3D, eight-node, reduced integration elements (ABAQUS element type C3D8R) for the core. Ultimately, the analytical results were found to conform "fairly well" to the ABAQUS model (See Figure 2.5 for an example, where "critical impulse" was used as a metric for comparison of analytical results to FEA).

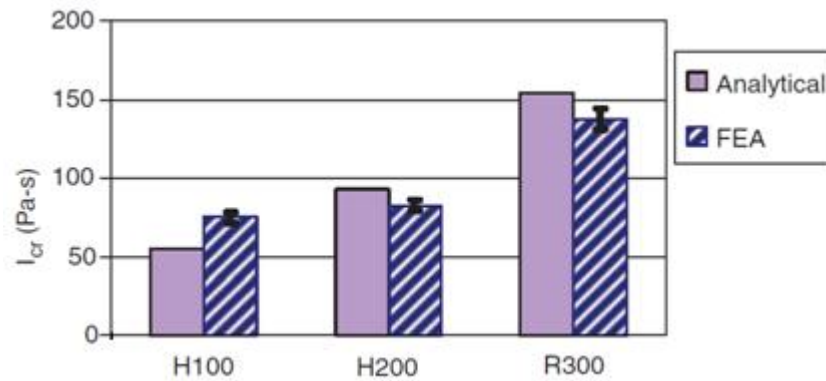


Figure 2.5: Variation of critical impulse of failure with varying core material properties (Hoo-Fatt and Palla 2009)

2.4 Work Post-Helmstetter

Other recent, topical work also relates to foam-core composites. Li et al. (2004) discussed the effects of the ratio of facesheet thickness (h_f) over core thickness (h_c) regarding panel design. It was found that as h_f/h_c increases, the maximum value of the displacement at the center of the top facesheet decreases. The work advised that h_f/h_c should not be less than a critical value for the design criterion (e.g. maximum transverse deformation) while remaining as small as possible. Such a comparison may serve as a useful future frame of reference for recommended design criteria.

2.5 Conclusions

Literature on utilizing advanced composites for blast mitigation focuses on facesheets separated by foam cores. Optimized core geometries for anything but foam core composite sandwich panels remain as unresearched as they did during Helmstetter's work on the project (2009). Foam core composites are more realistic than panels without foam. However, a combination of web stiffener and foam core panels is likely the best alternative. In this work, the foam is omitted as a

simplification. Hopefully, research on the topic of stiffener design can work in tandem with work in foam composites.

Chapter 3

MODELING BLASTS

3.1 Introduction

The fundamentals of blast modeling used herein stem from Gilbert Kinney and Kenneth Graham's *Explosive Shocks in Air*, published in 1985. Kinney and Graham's text presents governing equations that enable calculation of key parameters necessary to model a chemical explosion. Chapter 3 therefore explains these equations, their underlying theory, and how this leads to meaningful input for finite element software.

3.2 Blast Effects

Explosions, in essence, are sudden releases of energy (Kinney & Graham 1). However, chemical explosions and nuclear explosions are modeled differently. As this project seeks to mitigate the effects of blasts caused by chemicals such as TNT or ammonium nitrate rather than those caused by nuclear weapons, this chapter explores models of chemical explosions. Nuclear weapons, while far more disastrous, have remained unused by an aggressor since "Fat Man" wreaked havoc on Nagasaki during World War II. By contrast, chemical explosives are far more common and much more likely to be used by an aggressor to assault a victim, thus justifying this project's scope.

Common knowledge holds that an ignited explosive will create a destructive "push" on the atmosphere in the vicinity of the explosion. When speaking

in terms of blasts, the explosive is known as the “charge,” and the “push” on the atmosphere is known as a “blast wave.” As energy is rapidly released from the charge, the gases produced by the explosion forcefully propel the surrounding atmosphere away from the charge. Common knowledge also understands that larger charges will produce greater blast waves and that the magnitude of the blast wave will dissipate as one moves further away from the charge. These parameters are known as charge size and standoff distance, respectively, and provide a sizeable amount of the data needed to sketch a blast profile.

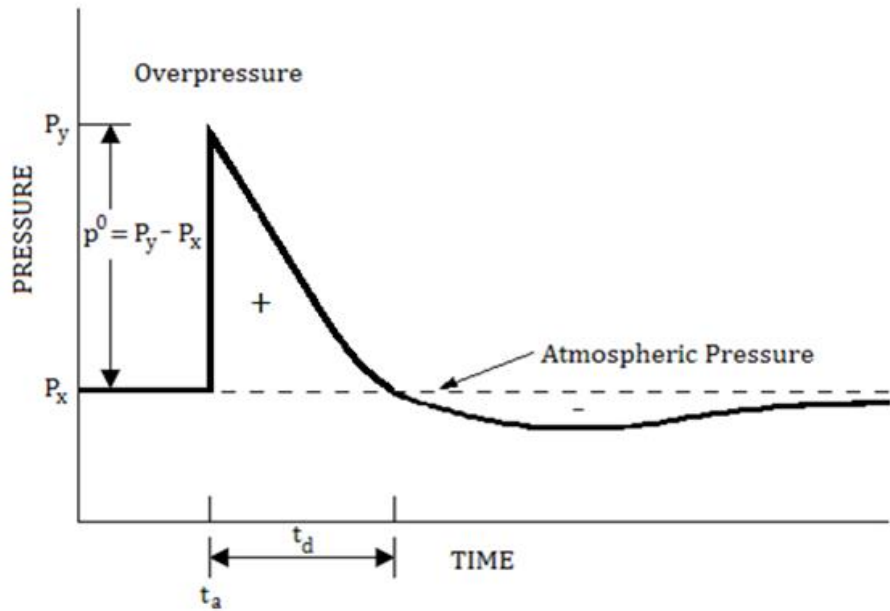
As a variety of materials may serve as a charge, logic dictates that governing equations should be derived relative to one particular type of explosive. The equations presented in Section 3.2.2 hold for 2,4,5-trinitrotoluene, colloquially called TNT. As TNT is stable and pure, meaning it can be handled easily and behaves reliably in multiple experiments. Therefore, it emerged as the basis upon which to base the blast equations and the potential of other types of chemical explosives. Other explosives are usually assigned a TNT equivalence, which quantifies the magnitude of an explosive’s energy release relative to an equivalent quantity of TNT. One gram of TNT releases 4610 J upon detonation.

3.2.1 Pressure-versus-Time Relationships

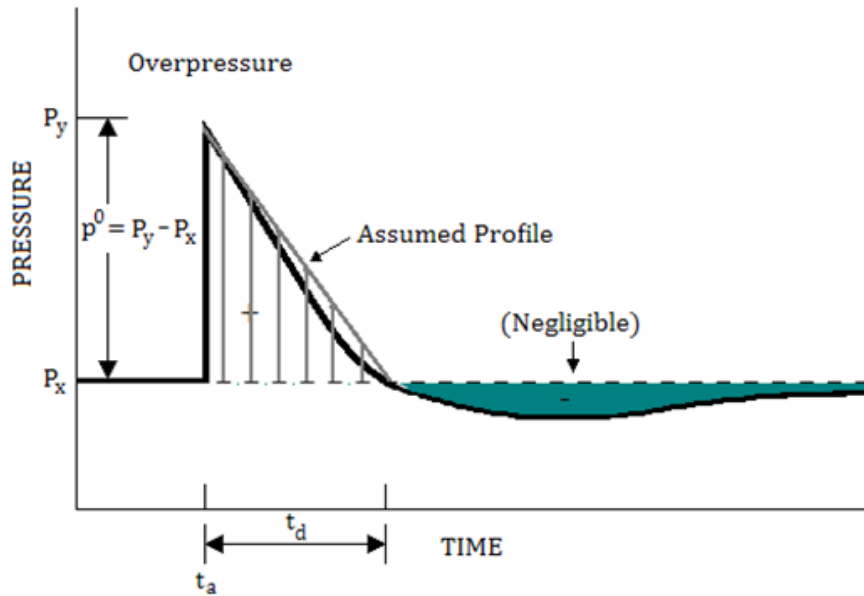
In the most basic sense, an explosive is effective because it creates a surcharge pressure above ambient atmospheric pressure very rapidly. At a given standoff distance, the pressure-versus-time profile resembles Figure 3.1a. Imagine a point that lies some known standoff distance away from a charge. After detonation (time zero), a very small amount of time will pass (on the order of milliseconds) before the blast wave strikes a point. This is the arrival time (denoted by t_a). Instantly

thereafter, the pressure felt by the point will escalate to the peak overpressure (denoted by p^0), caused by blast wave propagating toward and finally striking the point.

However, such a rapid overpressure creates a severe imbalance. The overpressure will decay exponentially below ambient atmospheric pressure until it reaches a negative pressure, which is something of a rebounding to compensate for the rapid overpressure caused by superheated gases. The period of time in which the curve lies above ambient atmospheric pressure is known as the duration of the positive phase (denoted by t_d).



(a)



(b)

Figure 3.1: Pressure versus time profile: (a) theoretical curve and (b) distribution assumed herein

By inspection, the positive pressure caused by the instantaneous spike in pressure is far more intense, and therefore much more damaging, than the negative pressure phase. Figure 3.1b illustrates the approach to blast profiles utilized in this project. The triangular, shaded positive region supplies enough information to simulate a blast reasonably.

3.2.2 Pressure-versus-Time Equations

Figure 3.1 shows that three parameters can appropriately describe a blast: peak overpressure, blast duration, and arrival time. This section enumerates the equations by which these parameters are obtained. All equations are reproduced from Kinney and Graham's (1985) text. Note that all equations herein typically take *Système Internationale* units as inputs. The project itself has largely made use of Imperial units, therefore necessitating careful conversion and unit consciousness when utilizing the equations.

Equation 3.1 equates the ratio of overpressure to atmospheric pressure to a cumbersome expression in terms of Z , the scaled distance (Equation 3.2).

$$\frac{p^0}{P_a} = \frac{808 \left[1 + \left(\frac{Z}{4.5} \right)^2 \right]}{\sqrt{1 + \left(\frac{Z}{0.048} \right)^2} \sqrt{1 + \left(\frac{Z}{0.32} \right)^2} \sqrt{1 + \left(\frac{Z}{1.35} \right)^2}} \quad (3.1)$$

$$Z = \frac{f_d \times \text{actual distance}}{W^{\frac{1}{3}}} \quad (3.2)$$

$$f_d = \left(\frac{\rho}{\rho_0} \right)^{1/3} = \left(\frac{P}{P_0} \right)^{1/3} \times \left(\frac{T_0}{T} \right)^{1/3} \quad (3.3)$$

In Equations 3.1 and 3.2, p^0 is the peak overpressure, P_a is atmospheric pressure, Z is the scaled standoff distance, f_d is an atmospheric transmission factor (expressed in Equation 3.3 in terms of atmospheric pressures and temperatures), and W is the mass of TNT.

The ratio of positive phase duration over mass of TNT (Eq. 3.4) is similar to the ratio of overpressure over atmospheric pressure in that it is dependent upon a complicated expression taking scaled standoff distance as the sole parameter.

$$\frac{t_d}{W^{\frac{1}{3}}} = \frac{980 \left[1 + \left(\frac{Z}{0.54} \right)^{10} \right]}{\left[1 + \left(\frac{Z}{0.02} \right)^3 \right] \left[1 + \left(\frac{Z}{0.74} \right)^6 \right] \sqrt{1 + \left(\frac{Z}{6.9} \right)^2}} \quad (3.4)$$

$$Z = \frac{f_t \times \text{actual time}}{W^{\frac{1}{3}}} \quad (3.5)$$

$$f_t = f_d \left(\frac{a}{a_0} \right)^{1/3} \quad (3.6)$$

In equations 3.4 and 3.5, t_d is duration of the positive pressure phase, W is the mass of TNT, Z is the scaled duration, and f_t is an atmospheric transmission factor for time (expressed in equation 3.6, where a_0 is the speed of sound in the reference atmosphere and a is the speed of sound).

The final parameter needed is arrival time. With overpressure and atmospheric pressure already known, arrival time is given by the following integral:

$$t_a = \frac{1}{a_x} \int_{r_c}^r \left[\frac{1}{1 + \frac{6p^0}{7P_a}} \right]^{\frac{1}{2}} dr \quad (3.7)$$

where a_x is the speed of sound in the undisturbed atmosphere (340.4 m/s used herein), r is the distance from the center of the charge to the point of interest, and r_c is the radius of the charge. As charge radius appears in the integral, the shape of the charge matters. For the purposes of this project, the TNT is assumed spherical (*a la* the black bombs of cartoon fame), the geometry of which can be found by using the mass and density of TNT.

Equations 3.1 through 3.7 highlight the criteria necessary to obtain the key components of a blast. Mass of TNT and standoff distance are somewhat obvious. As the remaining factors all relate to the atmosphere in which the blast is occurring, altitude is the final necessary input. Values of P_a , f_d , and f_t for altitudes varying from 400 meters below sea level to 6000 meters above sea level come from a table, “The U.S. Standard Atmosphere,” in Kinney and Graham’s book (1985), and an altitude of zero (sea level) is assumed throughout this work.

3.3 MATLAB Modeling

Once a panel has been drawn in AutoCAD and mapped in FEMAP (as explained in Chapter 4), it must be loaded. The equations found in Section 3.2.2 provide the basis for modeling a blast load profile on a panel. MATLAB code was selected as an easy way to load the ABAQUS model. A series of programs written in MATLAB took standoff distance, mass of TNT, and altitude as inputs, calculated a peak overpressure (as a point load), arrival time, and duration for each node, and

printed the output in ABAQUS syntax in a diary file. Refer to Figure 3.2 for a graphical representation of the rationale.

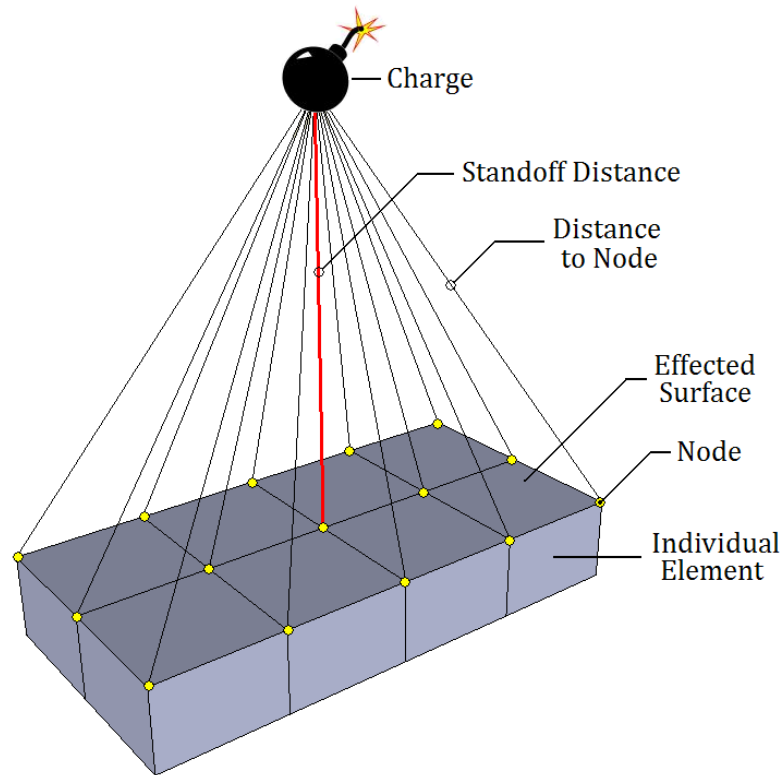


Figure 3.2: Generation of blast load on surface

ABAQUS accepts concentrated load input that varies in magnitude with time as follows:

time 1, normalized magnitude 1, time 2, normalized magnitude 2...

The normalized magnitude refers to dividing the magnitude of the concentrated load at its corresponding time by the magnitude of the concentrated load when it reaches its peak over the time interval. In that sense, the peak overpressure would have a normalized magnitude of 1 occurring at the arrival time. ABAQUS linearly interpolates the load between inputs. Refer to Figure 3.3 for a graphic representation of the meaningful data points (obtained as discussed in Section 3.2.2). At the instant

the charge detonates, the time is equal to zero and the normalized magnitude is equal to zero. Likewise, when the overpressure has peaked, the time is equal to the arrival time and the normalized magnitude is equal to one. The time “just before” arrival was determined by subtracting 10^{-6} seconds from the arrival time, which was judged to be a sufficiently small interval. Finally, when the positive pressure phase has ended, the time is equal to the arrival time plus the blast duration and the normalized magnitude is back down to zero.

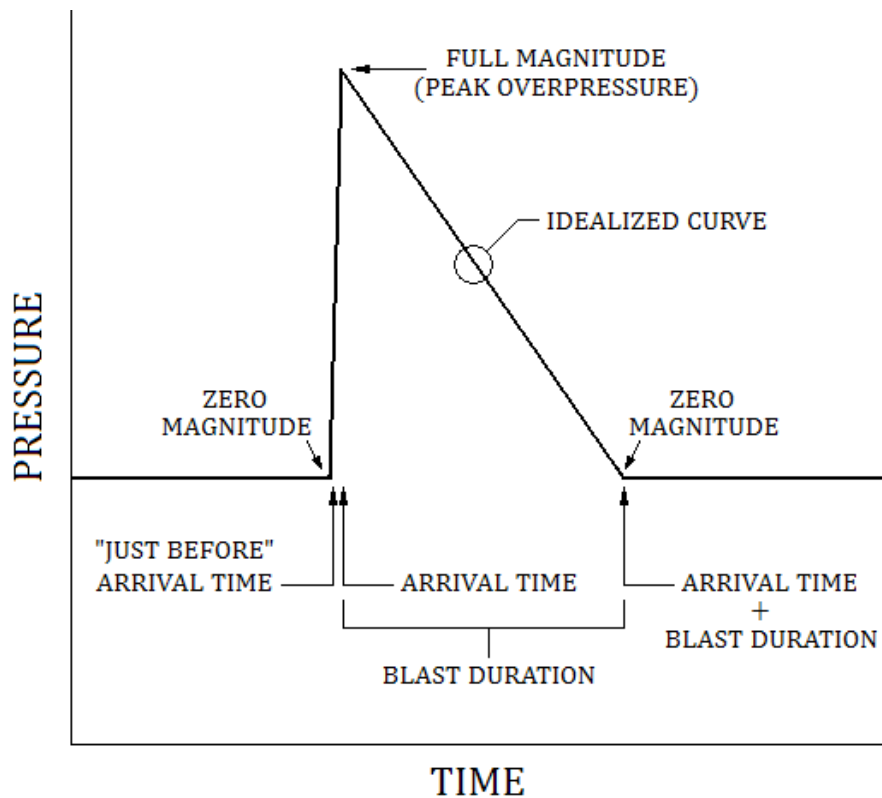


Figure 3.3: Parameters Needed to Write ABAQUS Load Input

From Figure X, it is evident that the profile can be described in ABAQUS syntax as follows:

0, 0, “just before” arrival time, 0, arrival time, 1, arrival time + blast duration, 0

The differing peak magnitude at each node is accounted for in a different portion of the ABAQUS model.

Therefore, if one can calculate the arrival time, blast duration, and overpressure for each point upon a panel's facesheet, one has a reasonably realistic profile to enter into ABAQUS for simulation. Figure 3.4 shows the schematic of MATLAB files that obtain those parameters from the inputs of mass of TNT, standoff distance, and altitude above sea level. MATLAB files may be found in Appendix A. The file BLAST.m is the highest level function m-file, which calls the other files and ultimately prints the data. The file tableXIV.m finds the atmospheric pressure and transmission factors for distance and time using a Table XIV in Kinney and Graham (1985). Equations 3.1, 3.2, 3.4, and 3.5 are applied by explosionOverpressure.m, scaledDistance.m, duration.m, and scaledTime.m, respectively.

Input: mass of TNT (W), standoff distance (Da), and altitude (Alt) above sea level

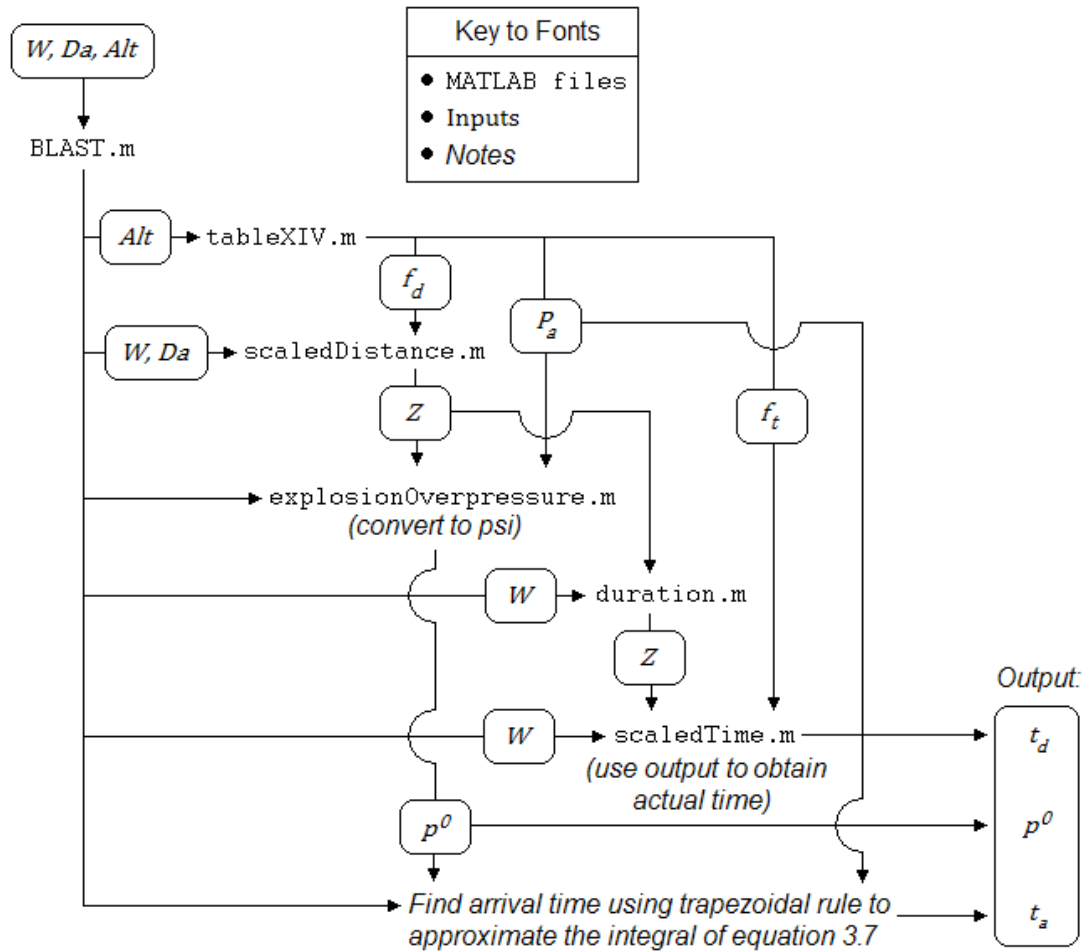


Figure 3.4: Schematic of MATLAB files used to generate outputs from inputs

Special files written for each panel analyzed (the different panels analyzed in the parametric study are discussed in Chapter 4) called the network of files in Figure 3.4 to obtain the load input for each node on each panel's surface, keeping mass of TNT and altitude constant but varying standoff distance for each node. The initial standoff distance is taken to be a dimension orthogonal from the center of the top facesheet, and varies for each node using the Pythagorean Theorem. Using a matrix of the top facesheet's node numbers, the programs then printed code in

ABAQUS syntax in diary files. The diary files may then be copied into the corresponding portions of the ABAQUS input file for amplitude data and concentrated load data.

Chapter 4

CONSTRUCTING FINITE ELEMENT MODELS

4.1 Introduction

The reader will find the methodology used to create the finite element models used to assess core geometries in this chapter. The general methodology is based on Helmstetter's research (2009), but makes several alterations to the model after the discovery of a significant input error. After addressing the error and exploring alternative modeling techniques to find a simulation with an equivalent deflection, the chapter then discusses the means taken to construct the models for the parametric study addressed in Chapter 5.

4.2 Model Generation

The following sections discuss model generation, which begins with generating the geometry, proceeds to mapping the model (stipulating the geometry of the finite element mesh), and ends with preparing the ABAQUS input files.

4.2.1 Drawing and Mapping

The seven models were drawn in AutoCAD for importation into FEMAP. After creating surfaces in FEMAP, stitching the surfaces into solid elements, defining material properties (Table 4.1), placing a finite element mesh of solids using "hex mesh solids," and placing a fixed boundary condition on the bottom facesheet, FEMAP then exported each model into ABAQUS input files.

The element dimensions varied for the facesheet elements and stiffener elements. Helmstetter (2009) suggested the facesheet and stiffener dimensions, based on a study by Lee et al (2004) suggesting a 5:1 facesheet thickness to stiffener thickness ratio. Therefore, the mesh size was chosen to accommodate the smallest dimension, which was the stiffener thickness of 0.05 inches. Facesheets consisted of elements that were 0.05 inches x 0.05 inches x 0.1 inches. The web stiffeners consisted of elements that were 0.05 inches x 0.1 inches x 0.1 inches. The mesh size was chosen to decrease the time needed to run the models.

The element type for all elements save for the brittle elements was *ELASTIC, TYPE=ENGINEERING CONSTANTS. This defines orthotropic behavior and allows the user to input elastic moduli, shear moduli, and Poisson's ratios in the principal directions (Dassault Systèmes 2007). The values for the aforementioned input may be found in Table 4.1.

In laboratory conditions the panel rested on a rigid surface and lateral movement was restrained using clamps. Therefore, the boundary condition was taken to be fixed along the bottom facesheet due to laboratory conditions (Helmstetter 2009).

The loads were input as concentrated loads with units of force using the *CLOAD command. Each *CLOAD can reference an amplitude, enabling the magnitude of the concentrated load to vary with time (as described in Chapter 3). The amplitudes and concentrated loads were generated using MATLAB and copied into the ABAQUS analysis file.

Table 4.1: Material properties for FEM input file

Material Properties			
Elastic Modulus (psi)			
	E₁	E₂	E₃
Facesheets:	3673806	3673806	1952208
Stiffeners:	3440000	3440000	1800000
Shear Modulus (psi)			
	G₁₂	G₂₃	G₁₃
Facesheets:	752746	759998	759998
Stiffeners:	800000	435000	435000
Poisson's Ratio			
	ν₁₂	ν₂₃	ν₁₃
Facesheets:	0.12	0.29	0.29
Stiffeners:	0.324	0.28	0.28
Density (lb·s²)/in⁴			
Facesheets:	0.000175		
Stiffeners:	0.000112		

4.2.2 Imperfection Files

Mode shape files are used to implement geometric imperfections, which insures that that the stiffeners buckle as they likely will under a blast load. ABAQUS's *FREQUENCY, EIGENSOLVER=LANCZOS command was used to create imperfections by performing modal analyses of the structure using eigenvalue extraction to calculate the natural frequencies and the corresponding mode shapes. In most cases, specifying ten mode shapes insured that one of them matched a likely deformed shape, representing initial imperfections of the model (Helmstetter 2009). The facesheet/stiffener interface was modeled using *MPC and PIN connections for the mode shape file. Physically, this represents a multi-point constraint with pin connections between nodes. This makes the global displacements equal, but leaves the rotations (if they exist) independent of each other (Dassault Systèmes 2007).

4.3 Helmstetter's FEM

Helmstetter investigated several different alternative modeling techniques, ultimately selecting a model that best fit his experiments as described in Helmstetter 2009. The analysis file contained CONN3D2 elements (a connection between two elements analyzed in three dimensions with all six degrees of freedom) at the web stiffener/facesheet interface to simulate the reduction in stiffness due to delamination at this interface, as observed in a high-speed video of the experiment.

Material properties and connection properties used during the early phase of this project matched Helmstetter exactly. However, further review of Helmstetter's finite element code revealed that the density input was a weight density rather than a mass density. As ABAQUS has no units of its own – rather, one must use a consistent set of units – absolute uniformity must be carefully checked. The original input of lb/in^3 not only needs to be divided by gravity, but gravity with units of in/s^2 to maintain the integrity of pounds and inches:

$$1 \text{ lbf} = 1 \text{ lb} * 32.2 \frac{\text{ft}}{\text{s}^2} = 1 \text{ lb} * 386.4 \frac{\text{in}}{\text{s}^2}$$

This oversight necessitated changes in the construction of the model. The CONN3D2 elements which affixed the tops of the stiffeners to the blast-absorbing facesheet did not supply adequate stiffness to model Helmstetter's point-load ABAQUS load case once the decreased density was correctly input.

Removing the CONN3D2 elements required an exploration into alternative connections modeling at the interface between the tops of the stiffeners and the bottom of the top facesheet. A simple solution to boost the panel's stiffness was to model it as a fixed connection, merging coincident nodes.

Bulk viscosity, brittleness, and mode shape alterations were also tested in ABAQUS. Bulk viscosity had hitherto been left at its default setting. Some

exploration into its effect on the model was explored by doubling it and adjusting it to compensate for density (it was ultimately deemed inapplicable in this case). Prior to focusing on discerning an appropriate model, the exact form of the brittle command was another frontier of this project. With stiffeners that are much less dense, the possibility of ignoring the brittle command was also explored. Finally, differences were observed if the mode shape files were varied. A summary of results can be seen in Table 4.2. The comparison was the 94 J experiment in Helmstetter (2009). Time constraints limited comparisons to the 151 J experiment (Helmstetter 2009).

Table 4.2: Deflections for alternative modeling strategies

Control	Maximum Deflection (inches)	Percent Difference
94 J Experiment	0.7	N/A
Analytical Models	Maximum Deflection (inches)	Percent Difference
Original Model with Incorrect Density	0.289	58.68%
Original Model with Corrected Density	0.949	35.60%
Fixed connections between stiffeners and facesheets Stiffeners have no brittle portions Fixed connection mode shape	0.826	18.03%
Fixed connections between stiffeners and facesheets Stiffeners have no brittle portions Bulk viscosity 1 is doubled while bulk viscosity 2 remains unchanged	0.826	18.02%
Fixed connections between stiffeners and facesheets Stiffeners have no brittle portions Bulk viscosity 2 is doubled while bulk viscosity 1 remains unchanged	0.826	18.03%
Fixed connections between stiffeners and facesheets Stiffeners have no brittle portions Bulk viscosity 2 compensates for density while bulk viscosity 1 remains	0.829	18.38%
*JOIN command on the stiffener-facesheet interface Stiffeners have no brittle portions *JOIN mode shape	0.921	31.64%
Fixed connections between stiffeners and facesheets All stiffeners save for the outermost have brittle centers Fixed connection mode shape (mode 10)	0.781	11.55%
Fixed connections between stiffeners and facesheets All stiffeners have brittle centers Fixed connection mode shape (mode 10)	0.601	14.14%
Fixed connections between stiffeners and facesheets All stiffeners have brittle centers Original model mode shape (mode 10)	0.763	8.98%

4.4 Selected Analysis File

The analysis file references an imperfection file with multi-point constraint pins. As in Helmstetter's model, the C3D8 elements were changed into C3D8R (continuum 3D, 8 node, reduced integration) elements for the ABAQUS input file itself. Brittle commands were applied to elements at the center of each panel to insure they failed (Helmstetter 2009). As the panels were to be elongated and the geometries were to vary, brittle commands were applied to the centermost elements of all the stiffeners. This is the modeling technique used in the analysis described by the last entry in Table 4.2.

Chapter 5

PARAMETRIC STUDY

5.1 Introduction

This chapter discusses the comparison of various core geometries, a key element that Helmstetter (2009) mentioned in his assessment of future research. The results of the parametric study are presented and interpreted by several metrics. The moment transferred through the panel is fitted to a nonlinear equation to gain a rough idea of the effect of stiffener height and stiffener spacing.

5.2 Parameters

Throughout the project, the thicknesses of the facesheets, the thicknesses of the stiffeners, and the overall depth of the panel element in question were all kept constant (at 0.25 inch, 0.05 inch, and 2.0 inches, respectively). Therefore, the variables to be studied were web spacing (S_w), height (H), and therefore the ratio between the two (S_w/H).

Early in the project, the varying heights and stiffener spacings presented in Table 5.1 were selected for evaluation. Notably, the model corresponding to $H = 1$ inch and $S_w = 1.5$ inches (bolded in Table 5.1) matches the stiffener configuration of Helmstetter's model. From there, spacing and heights were chosen to create stiffener spacings varying from 1 inch to 3 inches, and stiffener heights varying from 0.75 inch to 2 inches. In most models, each height or spacing can be compared to another model in which one of those values is the same and the other varies (this is not true at the

limits of the ranges of the parameters, where only one model exists with $S_w = 1$ inch and one model exists for $H = 2$ inches). Additionally, three values of S_w/H (1.333, 1.5, and 2.0) facilitate comparisons of panels with the same ratio and enables exploration into the effect of that variable.

Table 5.1: Web spacings, heights, and S_w/H ratios investigated

		PARAMETRIC STUDY			
		Web Spacing, S_w (in)			
Height (in)		1	1.5	2	3
	0.75	1.333333	2	-	-
	1	-	1.5	2	-
	1.5	-	-	1.333333	2
	2	-	-	-	1.5

Throughout the remainder of the paper, the models will be referenced by a number. Starting in the top corner of Table 5.1 and moving from left to right, the models are numbered Model 1 through Model 7. For example, Model 2 has stiffer heights of 0.75 inch and spacings of 1.5 inches, while Model 3 has stiffer heights of 1 inch and spacings of 1.5 inches.

The model in Helmstetter (2009) contained facesheets that were 9 inches by 2 inches wide and 0.25 inches thick. The 2 inch width and 0.25 thickness remained for these models. The length was increased from 9 inches to 18 inches. This made the geometry a bit more manageable, as 18 is divisible by each of the web spacings. It also enabled the largest panel element to have the same number of stiffeners as Helmstetter’s model.

5.3 Loading

Table 5.2 shows equivalent weights of TNT for each panel's top facesheet that imparts a similar impulse to Helmstetter's 94 J test, which had an impulse of $6.8 \times 10^6 \text{ lb}\cdot\text{s}$. The MATLAB blast programs were modified to compute a total impulse from the overpressures and durations. The standoff distance was held constant and the charge size was increased by trial and error until the impulse was equivalent. The differences in charge size are due to slight differences (± 0.05) in the panel lengths from drawing them in AutoCAD.

Table 5.2: Equivalent TNT masses associated with Helmstetter's 94 J experiment

Model Number	Charge Size at 25 cm (9.84 in) Standoff Distance
1	47.19 kg (104.04 lb) TNT
2	47.03 kg (103.68 lb) TNT
3	47.03 kg (103.68 lb) TNT
4	46.74 kg (105.25 lb) TNT
5	47.11 kg (103.86 lb) TNT
6	47.03 kg (103.68 lb) TNT
7	47.03 kg (103.68 lb) TNT

As the blast load is distributed and the panels are twice as long, it would be difficult to compare the results to Helmstetter's model. The rapid nature of blasts made impulse more appropriate for the purposes of subjecting the panels to a similar loading event than equivalent force or some arbitrary combination of charge size and standoff distance.

5.4 Results

The following assessment section begins with a discussion of the models' accuracy. Then, the models are compared on several metrics, including total load under stiffeners, total moment along the bottom facesheet, equivalent stress (derived from moment), equivalent stress as a percentage of total load sustained, and equivalent stress normalized by volume. The moment and equivalent stress would likely be future design parameters. The other metrics are ways of comparing each panel's efficacy to the others in terms of load mitigation (when compared to total load sustained) and economics (when compared by volume).

5.4.1 Deformed Shape

While the input connections at the stiffener/facesheet interface seemed to hone the deflection output from the finite element model within a decent percentage of the actual deflection for the purposes of a parametric study, it should be noted that a blast load delivering identical impulse did not produce a similar deflected shape. The stiffeners buckled and fractured immediately after the onset of the load. The stiffeners fractured in the first frame of the analysis. The time step corresponding to the first frame for each model is shown in Table 5.3. Therefore, the analyses presented herein are probably insufficient for practical use, but are still an effective tool in the search for a geometric optimum.

Table 5.3: Time step of initial frame

Model	Time Step
1	1.0005 E-04
2	1.0001 E-04
3	1.0001 E-04
4	1.0000 E-04
5	1.0001 E-04
6	1.0004 E-04
7	1.0000 E-04

5.4.2 Total Loads at Stiffener Bases

After the stiffeners buckled, the total loads at the bases of the stiffeners were probed in ABAQUS. Each stiffener was one element thick (0.05 inches) and 20 elements deep (each being 0.1 inches). The maximum principal stress was obtained from each element's centroid. It was assumed that the majority of the stress would be axial at the stiffeners' bases. Refer to Table 5.4 to see that the value used herein (maximum principle) was largely driven by S_{33} . The sum of all 20 stresses from each stiffener can then be multiplied by the stiffener's cross-sectional area to get a point load at each stiffener location, which is imparted into the bottom facesheet. The sum of all the stiffeners present in an 18 inch length of panel represents the total load that is being imparted into the bottom facesheets, which in turn are assumed fixed to the structure the panels are protecting (this may not exist in reality, but as the laboratory tests were fixed, it is the only boundary condition that can be used for comparison). Figure 5.1 presents these results as a bar graph, showing $S_w/H = 1.333$ inches light gray, $S_w/H = 1.5$ inches dark gray, and $S_w/H = 2$ inches black.

Table 5.4: Stress values from ABAQUS probe for a sample element

Stress Output	Stress (psi)
Max. Principal:	21416.7
S ₁₁ :	-521.828
S ₂₂ :	561.614
S ₃₃ :	21403.1
S ₁₃ :	28.1055
S ₁₂ :	-499.53
S ₂₃ :	-215.696

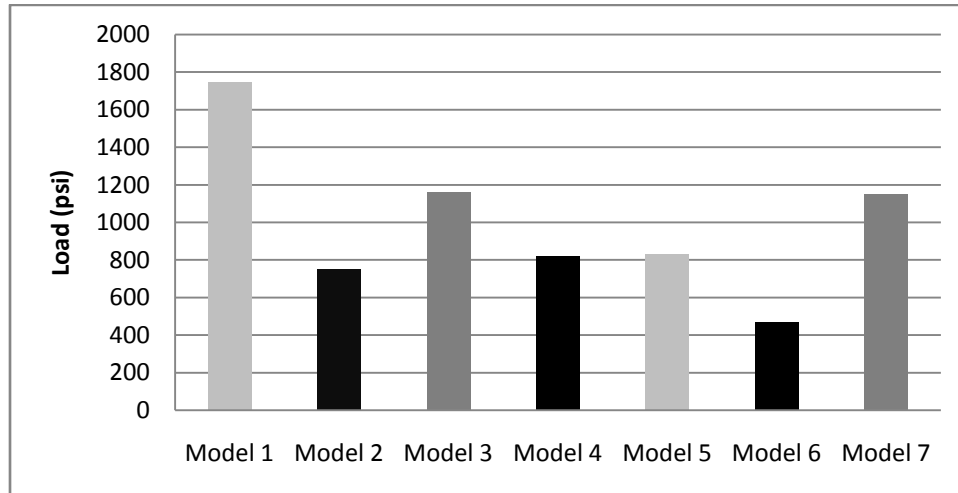


Figure 5.1: Sum of stresses in bottom elements at stiffener bases.

The magnitude of the load obtained from element probing probably does not paint the most accurate portrait of model efficacy. The following sections assess the panel behavior by other metrics.

5.4.3 Maximum Moment

While a summation of point loads sustained over the 18 inch sections of panel provides a quick idea of the load imparted into the protected structure, it does

not paint an entirely accurate picture the panel's efficacy. After the stiffeners buckle, the bottom facesheet can be thought of as a beam with the point loads at the stiffener bases as the load. In that sense, a moment diagram may be obtained for each panel. Figure 5.2 shows the seven moment diagrams graphed against each other. From 5.2, one will note that Models 2, 4, and 6 ($S_w/H=2$) all have the lowest profiles, with Models 4 and 6 appearing nearly like reflections of each other. Figure 5.3 shows the maximum moment for each model.

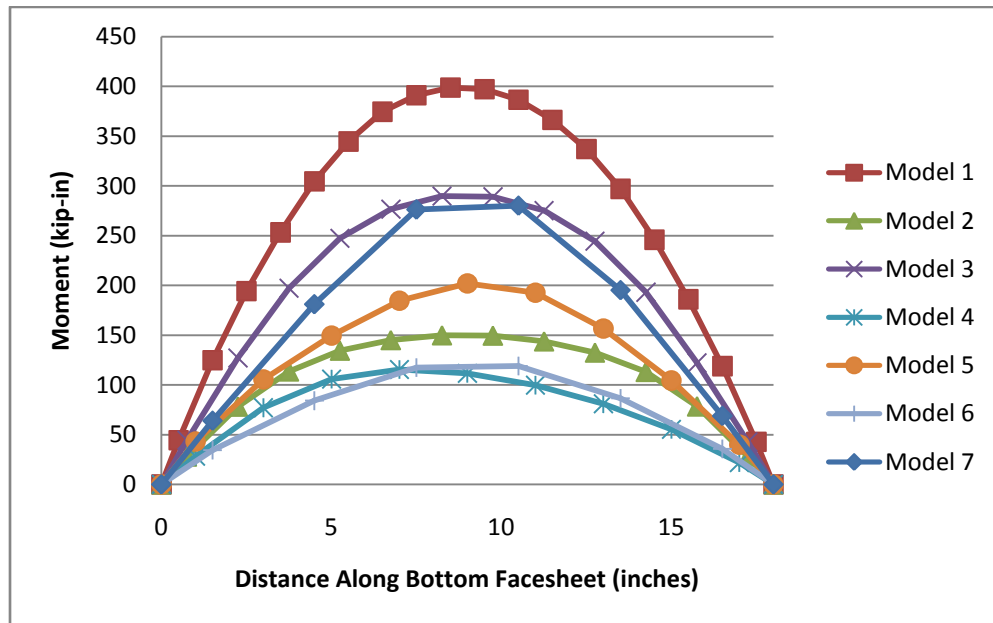


Figure 5.2: Moment along bottom facesheet due to stiffener loads

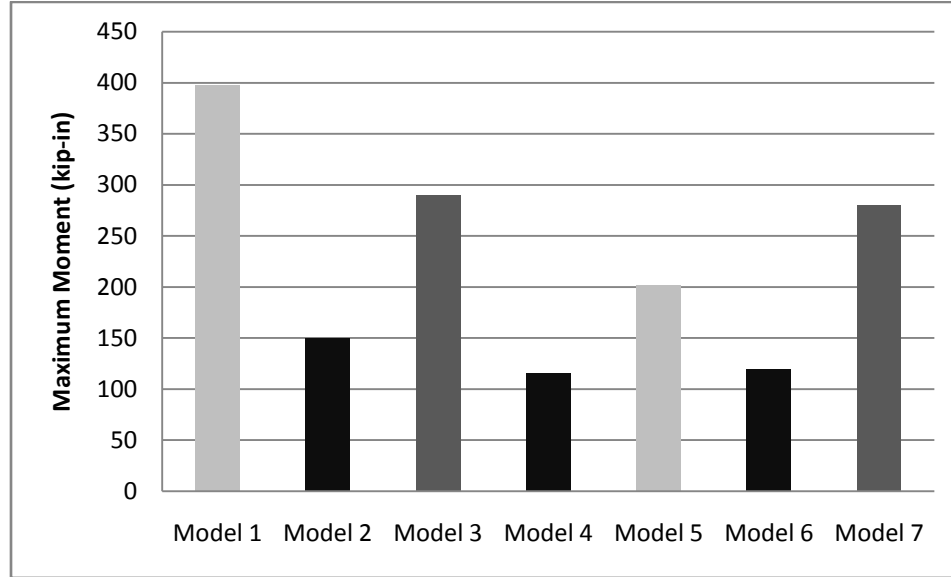


Figure 5.3: Maximum moment at bottom facesheet

5.4.4 Total Reaction

Another important factor that will play an important role in panel design will be a protected structure's ability to supply a reaction stress to the panel's bottom facesheet in order to maintain equilibrium. Figure 5.4 expresses this concept. Each point load, P , was obtained by summing the stresses probed from ABAQUS as described in Section 5.4.1. P represents the sum of centroidal element stresses resolved over the area. The maximum moment was obtained by simple static analysis of the bottom facesheet. An equivalent uniformly distributed load, w , can be obtained from the maximum moment by the following equation:

$$\frac{wL^2}{8} = M_{max} \quad (5.1)$$

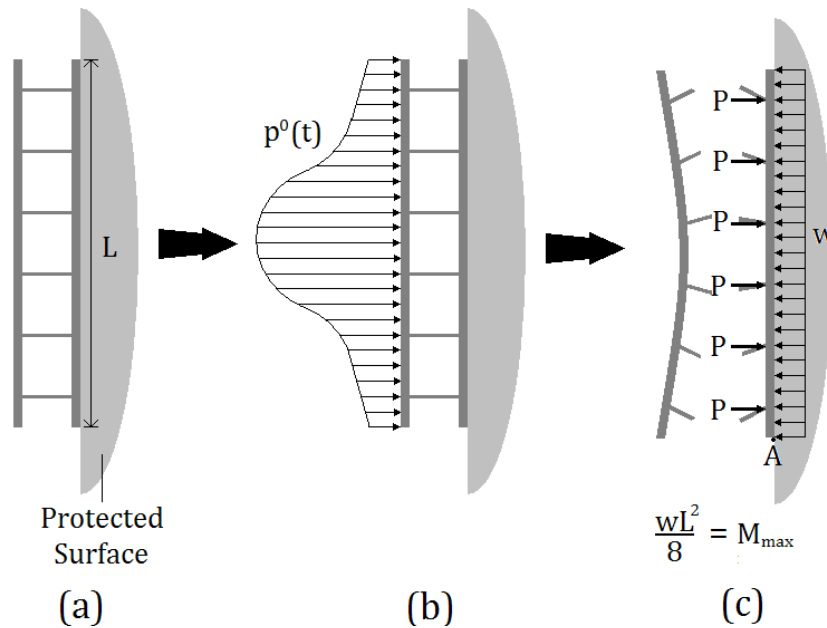


Figure 5.4 Method of obtaining a distributed load

As the pressure is not in fact uniform, the value for w is an approximation used for comparison. Once obtained, the seven uniformly distributed pressures calculated behind the bottom facesheet were graphed in Figure 5.5.

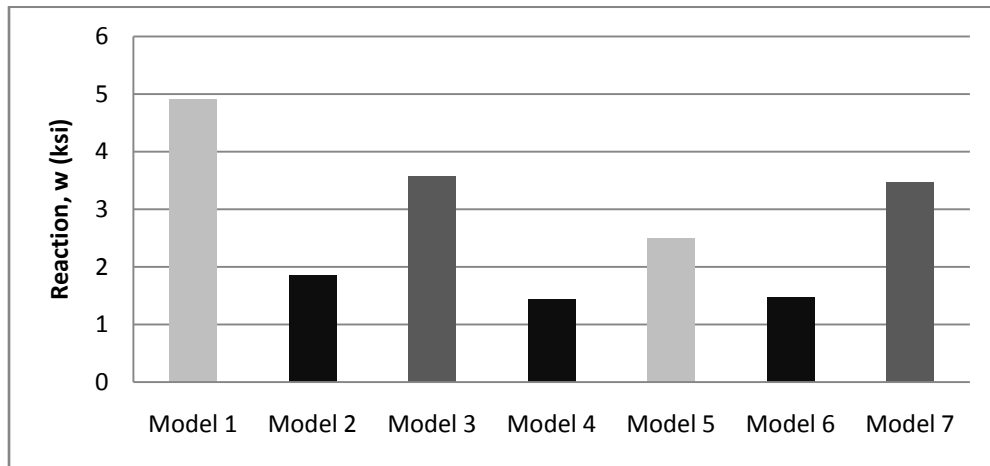


Figure 5.5: Approximate magnitude of reaction stress at bottom facesheet necessary for static equilibrium

5.4.5 Total Reaction Normalized by Total Blast Overpressure

Another metric for studying a model's efficiency is the factor by which it reduces the magnitude of the peak overpressure. The MATLAB codes that loaded the models were modified to obtain a total load for each panel by summing the matrix of overpressures (magnitudes shown in Table 5.5). The small differences in peak overpressure magnitude in the table are due to slight variation (+/- 0.05 inches) in panel length which occurred when the models were drawn in AutoCAD (as part of the researcher's learning curve). The total percentage by which each panel reduces the load is shown in Table 5.5 and graphed in Figure 5.6. The values for the reaction in Table 5.5 are calculated from the maximum moment as described by Figure 5.5.

Table 5.5: Magnitudes of Overpressure for Each Model

Model	Peak Overpressure (ksi)	Reaction(ksi)	Percent Reduction
Model 1	216.57	4.90	97.74%
Model 2	218.46	1.85	99.15%
Model 3	218.46	3.58	98.36%
Model 4	219.13	1.43	99.35%
Model 5	217.89	2.49	98.86%
Model 6	218.46	1.47	99.33%
Model 7	218.46	3.46	98.42%

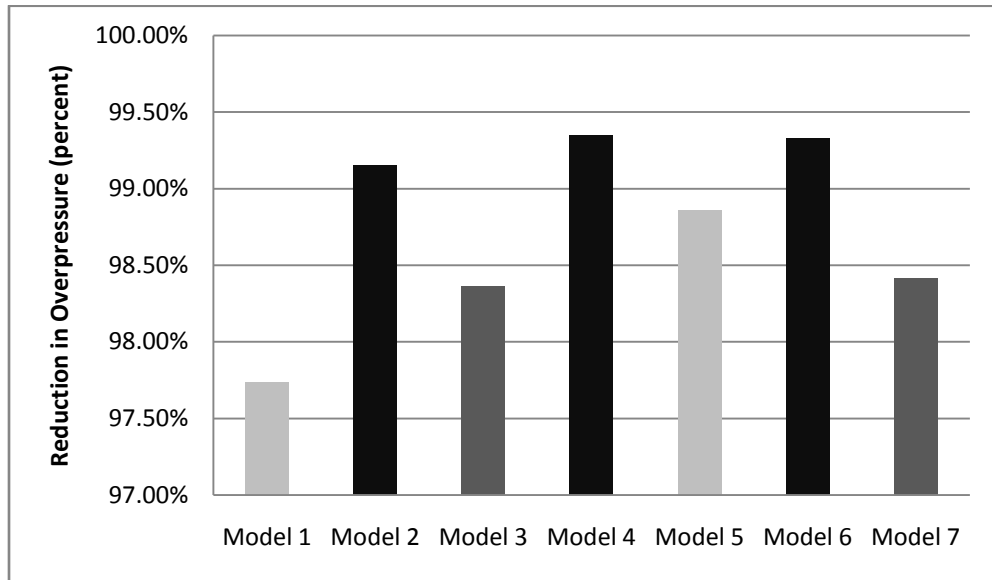


Figure 5.6: Percent reduction in peak overpressure

Figure 5.6 shows that the spread is small. The worst is above 97%, while all models with $S_w/H = 2$ reduce the overpressure by 99%. If peak overpressure is divided by the reaction (p^0/w), a load reduction factor can be obtained. Figure 5.7 presents that data. In this case, the spread is more defined. One can see that Model 4 reduces the load by a factor 100 times greater than Model 1.

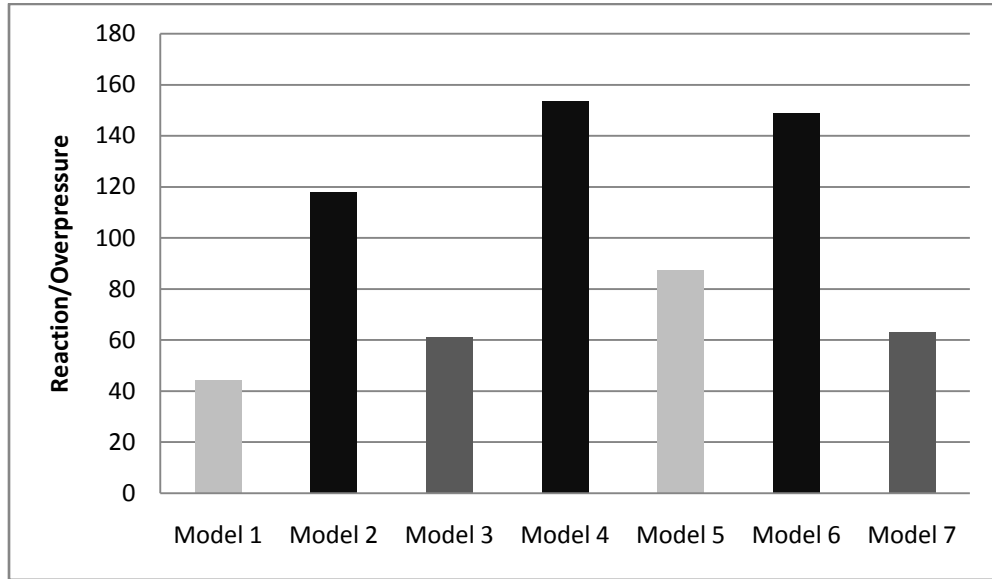


Figure 5.7: Overpressure Reduction Factor, Given by Reaction/Overpressure

5.4.6 Total Reaction Normalized by Core Volume

Another key parameter is determining an optimum value is economics, which for the purposes of panel design will be largely impacted by the amount of material used. Dividing by volume is thus a means to assess the efficacy of a given volume of panel when configured into the geometries studied. Table 5.6 shows the volumes of panels, while Figure 5.8 shows the reaction normalized by panel volume.

Table 5.6: Core Volumes

Model	Panel Section Volume (in³)
Model 1	1.35
Model 2	0.9
Model 3	1.2
Model 4	0.9
Model 5	1.35
Model 6	0.9
Model 7	1.2

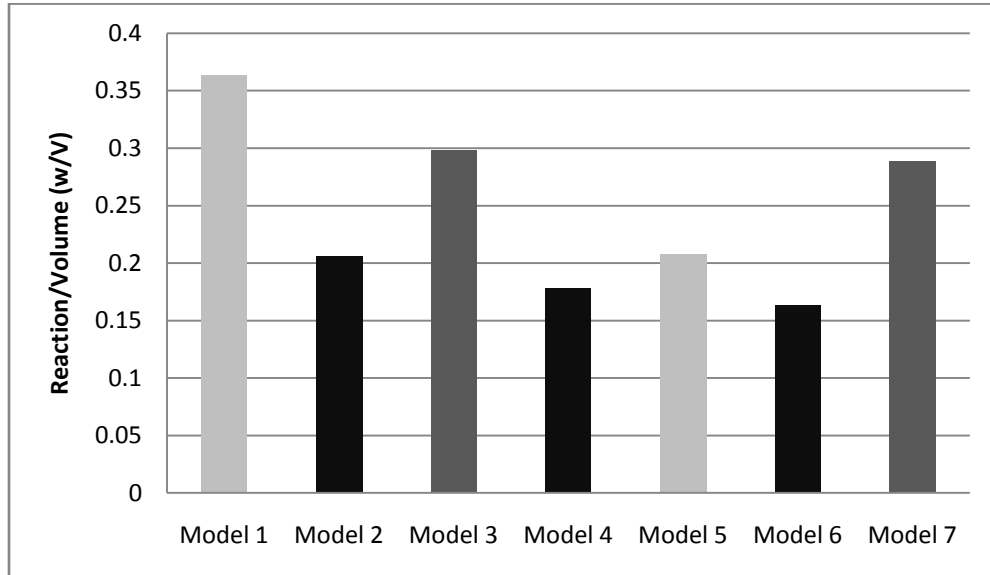


Figure 5.8: Reaction Normalized by Core Volume

5.5 Evaluation of Metrics

The criteria in Sections 5.4.1 to 5.4.6 are presented in Table 5.7 ranked by the geometry which performed the best in each category. For the reader's convenience, Table 5.8 presents model numbers and corresponding S_w/H ratios.

Table 5.7: Summary of Metrics Used to Assess Optimum Design

METRIC:	Total Load	Max. Moment	Reaction	p ⁰ Reduction, Percent	p ⁰ Reduction, Percent	w/V
Model Ranking	6	4	4	4	4	6
	4	6	6	6	6	4
	2	2	2	2	2	2
	5	5	5	5	5	5
	7	7	7	7	7	7
	3	3	3	3	3	3
	1	1	1	1	1	1

Table 5.8: Model numbers and corresponding S_w/H ratios

Model	S_w/H
1	1.33
2	2
3	1.5
4	2
5	1.33
6	2
7	1.5

Models with $S_w/H = 2$ occupy the top three positions by each metric. This was the highest ratio evaluated. Perhaps better performance could be obtained by further exceeding this. Additionally, while Model 4 ranks the highest in most categories, Model 6 is victorious in two very important categories: total load sustained and reaction normalized by volume. The latter metric is important in assessing efficiency, as it accounts for economics. Notably, Model 6 is also a boundary, as it has the largest web spacing (of 3 inches) with $S_w/H = 2$.

The lowest S_w/H ratio was 1.33, which was shared by Models 1 and 5. However, while $S_w/H = 1.5$ models behaved similarly to one another, a great disparity

was noticed between Model 1 and 5. While Model 1 was easily the worst, Model 5 offered greater resistance for any model with $S_w/H < 2$, going so far as to be nearly identical to Model 2 when normalized by core volume, suggesting there is potentially a significant benefit to the large web spacing (3 inches) of Model 5.

5.6 Data Analysis

The data suggests that the ratio of web spacing-to-height is an important parameter. An expression for the maximum moment as a function of simple geometric input like stiffener spacing and stiffener height would greatly reduce the complexity of analysis.

Assuming the ratio governs, the two should be related non-linearly by some equation in the form:

$$y = Kx_1^\alpha x_2^\beta \quad (5.2)$$

The sign of the exponents α and β will indicate if a ratio can be used as an indicator for optimum behavior. In this case, y would be the maximum moments, x_1 would be the stiffener spacing, and x_2 would be the stiffener height. The constant K and exponents α and β will be determined through matrix operations. Therefore:

$$M_{max} = K S_w^\alpha H^\beta \quad (5.3)$$

Taking the natural logarithm of both sides:

$$\ln M_{max} = \alpha \ln S_w + \beta \ln H + \ln K \quad (5.4)$$

In matrix form to accommodate the seven values:

$$\begin{bmatrix} \ln S_{w1} & \ln H_1 & \ln K_1 \\ \ln S_{w2} & \ln H_2 & \ln K_2 \\ \vdots & \vdots & \vdots \\ \ln S_{w7} & \ln H_7 & \ln K_7 \end{bmatrix} \begin{bmatrix} \alpha \\ \beta \\ \ln K \end{bmatrix} = \begin{bmatrix} \ln M_{max1} \\ \ln M_{max2} \\ \vdots \\ \ln M_{max7} \end{bmatrix} \quad (5.5)$$

Defining A, B, and C by as the following:

$$A = \begin{bmatrix} \ln S_{w1} & \ln H_1 & \ln K_1 \\ \ln S_{w2} & \ln H_2 & \ln K_2 \\ \vdots & \vdots & \vdots \\ \ln S_{w7} & \ln H_7 & \ln K_7 \end{bmatrix}, C = \begin{bmatrix} \alpha \\ \beta \\ \ln K \end{bmatrix}, \text{ and } B = \begin{bmatrix} \ln M_{max 1} \\ \ln M_{max 2} \\ \vdots \\ \ln M_{max 7} \end{bmatrix}$$

An equation for the vector C can be found using least-squares by:

$$C = (A^T A)^{-1} (A^T B) \quad (5.6)$$

The MATLAB script in Appendix A returned the following values:

$$\alpha = -2.2469$$

$$\beta = 1.9697$$

$$K = 645.43$$

Therefore, maximum moment as a function of stiffener spacing and height is given by:

$$M_{max}(S_w, H) = 645.43 \left(\frac{H^{1.97}}{S_w^{2.25}} \right) \quad (5.7)$$

The moment is therefore a surface in S_w and H . Figures 5.9 and 5.10 offer alternative views of the moment. Obviously, Equation 5.7 is specific to this particular load scenario. The constant K is likely a more complicated function of the load applied. Therefore, the equation is mostly helpful in ascertaining the effect of stiffener spacing and height. The output suggests that another data analysis performed after collection of more data points may make the ratio converge upon $(H/S_w)^2$ times some value that is a function of the load.

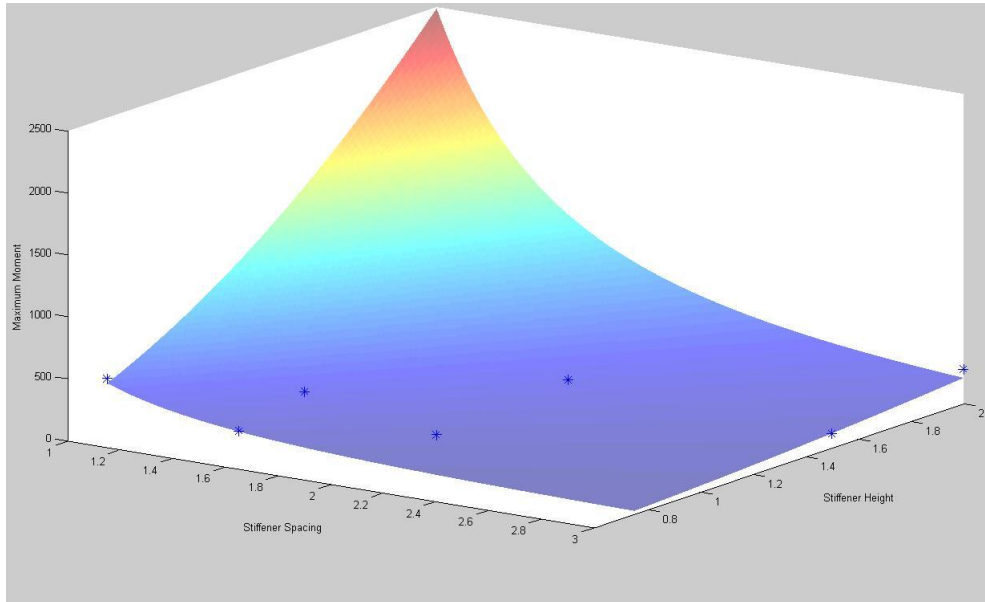


Figure 5.9: Surface Created by Equation 5.7

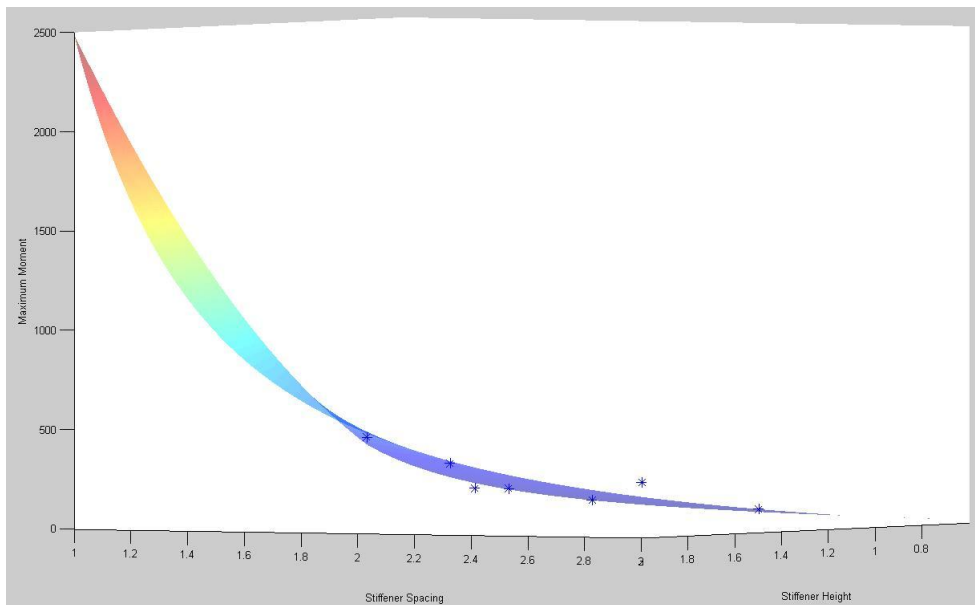


Figure 5.10: Surface Created by Equation 5.7 (Detail to Show Moments)

The figures show the probed moment values as asterisks straddling the surface. Obviously, the lower values of either parameter (e.g. heights or spacings

equal to zero) cannot be trusted, as either case effectively means a solid block of panel. Further work is necessary to determine the bounds of the equation.

5.7 Error Analysis

Table 5.9 shows the moment values obtained from Equation 5.7, the moments obtained through probing values from the ABAQUS model, and the percent difference. The high percent difference in Model 5 suggests further fitting work may show some other parameter which accounts for model performance. Figure 5.11 shows the graph of theoretical moment value versus the probed moment value to help assess the fit graphically. The error analysis gives an R^2 value of 0.748. The spreadsheet used to determine correlation may be found in Appendix B.

Table 5.9: Theoretical Moments, Probed Moment, and Percent Difference

Model No.	Fitted M_{\max} (kip-in)	Probed M_{\max} (kip-in)	% Difference
Model 1	360.57	397.27	9.24%
Model 2	144.99	149.92	3.29%
Model 3	255.51	289.70	11.80%
Model 4	133.87	115.58	15.82%
Model 5	297.53	201.93	47.34%
Model 6	119.63	118.97	0.56%
Model 7	210.84	280.11	24.73%

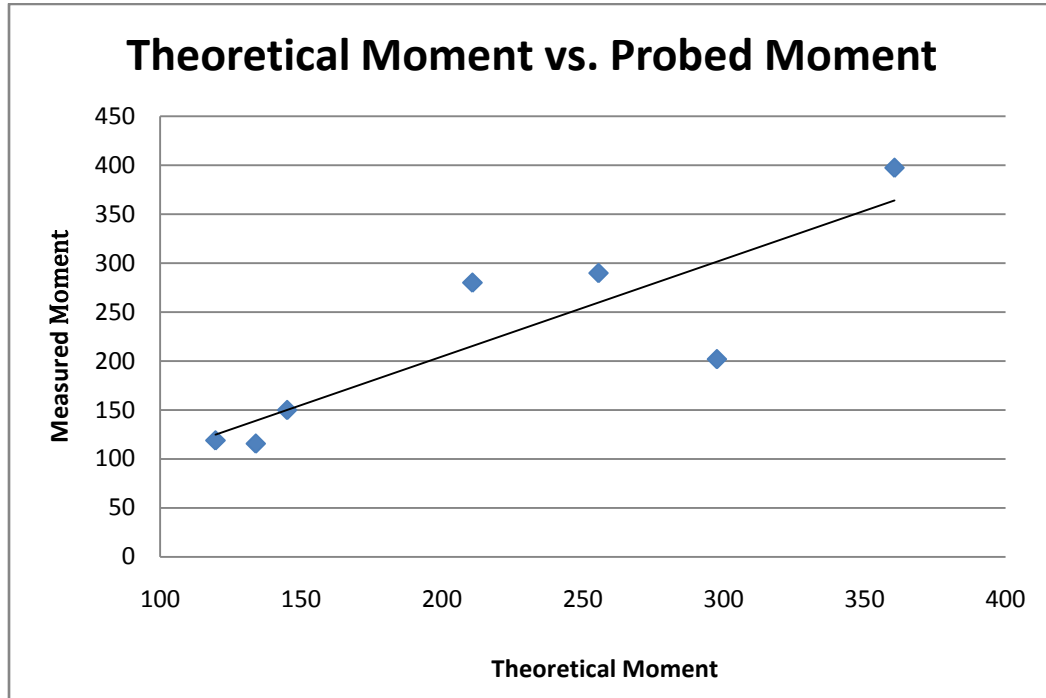


Figure 5.11: Correlation of Theoretical Moment to Probed Moment

5.8 Conclusion

Probing the ABAQUS models gave values for maximum principal stresses at the bases of each of the stiffeners. When manipulated to give point loads at the stiffener bases, the stress values were transformed into point loads along the bottom facesheet, which facilitated analyzing the bottom facesheet as a beam and finding a maximum moment along the panel's base. One can calculate a resultant pressure at the panel's base necessary to keep the panel in static equilibrium, which is in turn an approximation of the stress to which the protected structure is subjected. The stresses and moment values could then be compared to other criteria, such as blast overpressure and core volume. Using a nonlinear least-squares fit to the data, an equation was obtained to fit the moment as a surface above the plane of stiffener

spacing versus height. The values obtained by this equation correlate with an R^2 value of 0.748.

Models with a higher spacing-over-height ratio performed better under blast loading. Model 6 performed the best when compared to volume of material it uses in its core. Models with larger web spacing and web-to-height ratios would be necessary to discern whether efficiency would be further increased if these parameters were increased.

Chapter 6

CONCLUSIONS

6.1 Summary of Work

Threats of terrorist attack have motivated further investigation into sacrificial structures. Composite materials offer an innovative solution to the problem, given their high strength-to-weight ratios and ability to be fabricated into a variety of shapes. However, the complex nature of both composite mechanics and blast profiles makes analytical analysis of composite sandwich panels very difficult. Finite element software shows promise in panel analysis.

Blast and impulse load mitigation through composite sandwich panels has been researched for several years, and the literature on the topic is vast. However, as the variation in material properties and geometries is seemingly endless, the topic allows for plenty of avenues of exploration among researchers. A review of literature conducted in work by Helmstetter suggested more research should be done in panels constructed of facesheets separated by web stiffeners. Literature post-Helmstetter suggests that the topic of modeling these types of panels still leaves much to be desired, validating the need for further research.

The ability to generate a blast profile that comes near to simulating reality greatly advances the credibility of a finite element model meant to simulate a panel's behavior under a blast load. MATLAB was used to apply the complicated equations that govern blast behavior as described by Kinney and Graham, apply them to the

nodes on a panel surface, and print diary files that can quickly and easily be copied into ABAQUS input files.

The erroneous density present in Helmstetter's previous finite element model required a further study of modeling methodology. The study ultimately concluded that using mode shape files with pin connections atop the stiffeners and loaded models that use fixed connections atop stiffeners reproduces a deflection within 8% of Helmstetter's 94 J experiment. The parametric study models utilized this approach.

A parametric study was conducted to provide a series of models with varying stiffener spacing to stiffener height ratios for cross comparison. The parameters were studied under a simulated blast load due to a chemical explosion that imparts an equivalent impulse to Helmstetter's 94 J experiment.

6.2 Conclusions

Finite element models that do not deflect downward (as was observed herein) as expected may be questionable. While the models are not recommended for application in industry, they are assumed to be accurate enough for the purposes of a parameterized geometric analysis.

Among the models investigated, the models with S_w/H ratios equal to 2 consistently outperformed models with lower ratios. Several metrics were used to reach this conclusion. Perhaps the most important metric was the moment along the bottom facesheet, which was obtained by probing stress values in the bottom elements of the web stiffeners and treating the resultant force as a concentrated load acting along a beam. This moment could also be used to obtain an approximate distributed

load, which in turn can be compared to the peak overpressure (as the units are the same).

Web height divided by web spacing seems to be the most important parameter that affects blast mitigation potential. Specifically, a nonlinear least-squares analysis suggests that the moment at the base of a panel is dependent on $(H/S_w)^2$ times some function of the overpressure.

6.3 Future Work

Helmstetter's suggestions for future work included subjecting the finite element model to a realistic blast loading profile and conducting a parametric study, both of which were accomplished herein. However, other work suggested in the past remain unaddressed. No lab tests for determining accurate stiffnesses, poisson's ratios, and shear moduli of the stiffeners and facesheets were conducted. The bottom facesheet's boundary condition remained fixed rather than free to deflect, which overestimates the boundary condition stiffness assuming the panel is supported by a structural member with non-infinite stiffness.

No model validation under either a controlled chemical explosion or under a testing apparatus capable of impacting a nearly-equivalent load has been carried out for this work. An underlying reason for carrying out this study was the hypothesis that a finite element model that accurately simulates panel behavior under a point load impulse will also simulate panel behavior under a blast profile. Experiments of this nature would put this hypothesis into perspective.

The downward deflection of the top facesheet toward the bottom facesheet was not observed in the blast load analyses like it was in the Helmstetter's experiment and finite element model. This further suggests the need for experimental testing,

which would indicate whether the tendency of the top facesheets to ricochet back toward the charge as they did in the finite element models is accurate behavior or the result of a modeling error.

Furthermore, the facesheets are currently perfectly elastic. The high strain observed in the experiments certainly suggests that the facesheets eventually exhibit inelastic behavior.

Finally, more data points would validate Equation 5.7. Simply testing a model with an arbitrary stiffener spacing and height within the range tested here and comparing its maximum moment to the predicted value would shed light on its validity.

WORKS CITED

- Abaqus User Manual. (2007). Dassault Systèmes. Version 6.7. United States of America.
- Bahei-El-Din, Y. A., and G. J. Dvorak. (2007). "Behavior of Sandwich Plates Reinforced with Polyurethane/Polyurea Interlayers under Blast Loads." *Journal of Sandwich Structures and Materials*. Volume 9 pgs 261-281.
- Helmstetter, D.J. (2009). "Analysis Procedures for Optimizing the Core of Composite Sandwich Panels for Blast Resistance," Master's Thesis. University of Delaware.
- Hoo-Fatt, M.S., and L. Palla. (2009). "Analytical Modeling of Composite Sandwich Panels Under Blast Loads." *Journal of Sandwich Structures and Materials*. Volume 11 pgs 357-380.
- Kinney, G., and K. J. Graham. (1985). *Explosive Shocks in Air*. New York: Springer Verlag.
- Lee, D.K., and B.J. O'Toole. (2004). "Energy Absorbing Sandwich Structures Under Blast Loading," 8th International LS-DYNA Users Conference. Pgs. 8-13 – 8-24.
- Li, R., G.A. Kardomateas, and G.J. Simitse. (2009). "Point-wise Impulse (Blast) Response of a Composite Sandwich Plate Including Core Compressibility Effects." *International Journal of Solids and Structures*. Volume 46 pgs 2216-2223.

APPENDIX A: MATLAB FILES

Codes 1 through 6 are files that work together (as explained in Section 3.4) to load the top facesheets of the finite element models. Codes 7, 8, and 9 are examples of the codes that loaded individual models (shown here is model 1). Code 10 is a model that performed the matrix manipulations from Equation 5.6 in order to obtain Equation 5.7.

Code 1: BLAST.m

```
function blastData = BLAST(W, Da, Alt)

% BLAST(W, Da, Alt) finds the blast overpressure and duration of a
blast
% INPUTS (example):
%   W = mass of TNT, kg
%   Da = standoff distance, m
%   Alt = altitude, m
% OUTPUTS:
%   p0 = peak overpressure, psi
%   td = duration, milliseconds
%   ta = arrival time, seconds
% CALLS:
%   tableXIV.m
%   scaledDistance.m
%   explosionOverpressure.m
%   duration.m

% Find necessary parameters of the equation:
Pafdft = tableXIV(Alt);
Pa = Pafdft(1);
fd = Pafdft(2);
ft = Pafdft(3);
Z = scaledDistance(fd, Da, W);
rcharge = chargeRadius(W);
% Overpressure
p0 = explosionOverpressure(Pa, Z);
p0psi = p0*0.0145037738;
% Duration
scaledDuration = duration(Z, 1);
td = scaledTime(W, scaledDuration, ft);
```

```

% Arrival Time
OneoverMx = sqrt(1/(1+(6*p0)/(7*Pa)));
ax = 340.4; % m/s
ta = (1/ax)*(OneoverMx*Da - OneoverMx*rcharge);

% Create vector blastData for use in other programs
blastData = [p0psi td ta];

end

```

Code 2: tableXIV.m

```

function Pafdft = tableXIV(Altitude)

% (Table XIV, p. 259, Kinney & Graham, 1985)
% tableXIV(Altitude) finds the Pa, fd, and ft for a given altitude
% INPUTS:
%   Altitude = distance above/below sea level, m
% OUTPUTS:
%   Pa = U.S. Standard Atmospheric pressure, mbar
%   fd = Distance transmission factor at altitude, dimensionless
%   ft = Time transmission factor at altitude, dimensionless

% Round the altitude value to the nearest 200 m
roundFactor = floor(Altitude/200);
difference = abs(Altitude - 200*roundFactor);
if difference <= 100
    Altitude = Altitude - difference;
else
    difference2 = 200 - difference;
    Altitude = Altitude + difference2;
end

% Table XIV: The U.S. Standard Atmosphere (1976)
% [Altitude (m), Pressure (mbar), fd (Distance), ft (time)]
TableXIV = [-400 1056 1.011 1.016;
            -200 1038 1.007 1.09;
            0 1013.25 1.000 1.000;
            200 989 0.993 0.991;
            400 966 0.987 0.983;
            600 943 0.981 0.974;
            800 921 0.975 0.966;
            1000 899 0.968 0.958;
            1200 877 0.962 0.948;
            1400 856 0.956 0.940;
            1600 835 0.945 0.932;
            1800 815 0.943 0.923;
            2000 795 0.937 0.915;
            2200 775 0.930 0.907;
            2400 756 0.924 0.899;
            2600 738 0.918 0.891;
            2800 719 0.912 0.882;

```

```

3000 701 0.904 0.874;
3200 684 0.900 0.866;
3400 666 0.893 0.858;
3600 649 0.886 0.850;
3800 633 0.881 .0842;
4000 617 0.875 0.834;
5000 541 0.843 0.796;
10000 265 0.698 0.613];

for i = 1:25
    if Altitude == TableXIV(i,1)
        Pafdft = [TableXIV(i,2) TableXIV(i,3) TableXIV(i,4)];
        break
    elseif Altitude > 10000
        error('Altitude out of bounds')
    end
end

% * According to The Guinness Book of World Records, the highest town
in the world is Wenzhuan at altitude 5099.304 m
end

```

Code 3: scaledDistance.m

```

function Zd = scaledDistance(f,Da,W)

% (Eq. 7-4, Kinney & Graham, 1985)
% INPUTS:
% f = transmission factor (distance or time), dimensionless
% Da = actual standoff distance (m)
% W = equivalent mass of TNT (kg)
% OUTPUTS:
% Zd = scaled distance

Zd = (f*Da)/(W^(1/3));

end

```

Code 4: explosionOverpressure.m

```

function p0 = explosionOverpressure(Pa,Z)

% (Eq. 6-2, Kinney & Graham, 1985)
% explosionOverpressure.m calculates the peak overpressure needed for
the
% instantaneous overpressure decay function
% INPUTS:
% Z = scaled distance, from scaledDistance.m
% Pa = ambient atmospheric pressure
% OUTPUTS:
% p0 = explosion overpressure

```

```

numerator = Pa*(808*(1+(Z/4.5)^2));
denominator =
(sqrt(1+(Z/0.048)^2)*sqrt(1+(Z/0.32)^2)*sqrt(1+(Z/1.35)^2));
p0 = numerator/denominator;

end

```

Code 5: duration.m

```

function scaledDuration = duration(Z,W)

% (Eq. 6-10, Kinney & Graham, 1985)
% duration.m calculates the maximum duration of the blast for the
decay
% function
% INPUTS:
%   Z = scaled distance (from scaledDistance.m)
%   W = mass of TNT (kg)
% OUTPUTS:
%   td = duration of the positive pressure phase (milliseconds)

scaledDuration =
(W^(1/3))*(980*(1+(Z/0.54)^10))/((1+(Z/0.02)^3)*(1+(Z/0.74)^6)*sqrt(1
+(Z/6.9)^2));

end

```

Code 6: scaledTime.m

```

function td = scaledTime(W,scaledDuration,ft);

% (Eq. 7-9, Kinney & Graham, 1985)
% INPUTS
%   W = mass of TNT, kg
%   scaledDuration = scaled duration, milliseconds
%   ft = time transmission factor, dimensionless
% OUTPUTS
%   td = actual duration of the positive pressure phase
(milliseconds)

td = (W^(1/3))*(scaledDuration/ft);

end

```

Code 7: modellFlooding.m

```

function [] = modellFlooding(W, Da, Altitude)

% modellFlooding.m generates a point loads (from blast equations) for
% each surface node of the top face sheet Model 1:
% H = 0.75" Sw = 1.0 "
% INPUTS:

```

```

% W = mass of TNT, kg
% Da = standoff distance, m
% Alt = altitude, m
% OUTPUTS:
% Abaqus 6.71 code for a point load at each load using *CLOAD, psi

% (Conversions: 0.10 in = 0.00254 m & 0.05 in = 0.00127 m)

% MODEL INFO: For each row, there are 179 nodes
xNumberNodes=179;

% Find furthest distances in x and y (y constant for all models)
distx = xNumberNodes*0.00127; %
disty = 10*0.00254;

% English units for area - needed to find kips from ksi
Area = 0.1*0.05;
AreaMatrix = ones(xNumberNodes,11)*(Area);
side = ones(xNumberNodes,1)*(Area/2);
top = ones(1,11)*(Area/2);
AreaMatrix(:,1) = side;
AreaMatrix(1,:) = top;
AreaMatrix(1,1) = (Area/4);

% Find p0 for 1/4 of panel and use symmetry later
for i = 1:11
    for j=1:xNumberNodes
        yNodeDist = disty - 0.00254*(i-1);
        xNodeDist = distx - 0.00127*(j-1);
        nodeDistance = sqrt(sqrt(Da^2+yNodeDist^2)^2+xNodeDist^2);
        blastData = BLAST(W,nodeDistance,Altitude);
        p0psi(j,i) = blastData(1);
        td(j,i) = blastData(2);
        p0(j,i) = p0psi(j,i)*AreaMatrix(j,i);
    end
end

% make p0 map
p0Q2=fliplr(p0);
p0Q3=flipud(p0);
p0Q4=fliplr(p0Q3);
p0brillante=zeros(2*xNumberNodes-1,21);
p0brillante(1:xNumberNodes,1:11)=p0;
p0brillante(1:xNumberNodes,12:21)=p0Q2(1:xNumberNodes,2:11);
p0brillante(xNumberNodes+1:2*xNumberNodes,1:11)=p0Q3;
p0brillante(xNumberNodes+1:2*xNumberNodes,12:21)=p0Q4(1:xNumberNodes,
2:11);

for i=1:21
p0vector((i-1)*2*xNumberNodes+1:i*2*xNumberNodes,1)=p0brillante(:,i);
end

```

```

% Create proper ABAQUS output
for i=1:7518
    nodeList(i)=modellMatrix(i);
    fprintf('*CLOAD, OP=NEW, amplitude=Amp-%.0f\n',i)
    fprintf('%.0f,      2,      -%f\n',nodeList(i),p0vector(i))
end

end

```

Code 8: modellFtimedata.m

```

function [] = modellFtimedata(W,Da,Altitude)

% modellFtimedata.m creates a time profile (arrival/duration)
% each surface node of the top facesheet Model 2:
% H = 0.75" Sw = 1.0 "
% INPUTS:
%   W = mass of TNT, kg
%   Da = standoff distance, m
%   Alt = altitude, m
% OUTPUTS:
%   Abaqus 6.71 code time history suing *AMPLITUDE, seconds

% MODEL INFO: For each row, there are 179 nodes (half of total)
xNumberNodes=179;

% Find furthest distances in x and y (y constant for all models)
distx = xNumberNodes*0.00127;
disty = 10*0.00254;

% Find p0 for 1/4 of panel and use symmetry later
for i = 1:11
    for j=1:xNumberNodes
        yNodeDist = disty - 0.00254*(i-1);
        xNodeDist = distx - 0.00127*(j-1);
        nodeDistance = sqrt(sqrt(Da^2+yNodeDist^2)^2+xNodeDist^2);
        blastData = BLAST(W,nodeDistance,Altitude);
        td(j,i) = blastData(2)/1000;
        ta(j,i) = blastData(3);
    end
end

% Make td map
tdQ2=fliplr(td);
tdQ3=flipud(td);
tdQ4=fliplr(tdQ3);
tdbrillante=zeros(2*xNumberNodes-1,21);
tdbrillante(1:xNumberNodes,1:11)=td;
tdbrillante(1:xNumberNodes,12:21)=tdQ2(1:xNumberNodes,2:11);
tdbrillante(xNumberNodes+1:2*xNumberNodes,1:11)=tdQ3;

```

```

tdbrillante(xNumberNodes+1:2*xNumberNodes,12:21)=tdQ4(1:xNumberNodes,
2:11);

for i=1:21
tdvector((i-1)*2*xNumberNodes+1:i*2*xNumberNodes,1)=tdbrillante(:,i);
end

% Make ta map
taQ2=fliplr(ta);
taQ3=flipud(ta);
taQ4=fliplr(taQ3);
tabrillante=zeros(2*xNumberNodes-1,21);
tabrillante(1:xNumberNodes,1:11)=ta;
tabrillante(1:xNumberNodes,12:21)=taQ2(1:xNumberNodes,2:11);
tabrillante(xNumberNodes+1:2*xNumberNodes,1:11)=taQ3;
tabrillante(xNumberNodes+1:2*xNumberNodes,12:21)=taQ4(1:xNumberNodes,
2:11);

for i=1:21
tavector((i-1)*2*xNumberNodes+1:i*2*xNumberNodes,1)=tabrillante(:,i);
end

% Create data JUST BEFORE the arrival time to curb linear
interpolation
for i = 1:7518
    taminus(i) = tavector(i) - 0.000001;
end

% Create the point where the blast returns to zero
for i = 1:7518
totaltime(i) = tavector(i)+tdvector(i);
end

% MODEL INFO: 7518 nodes for the top facesheet
for i = 1:7518
fprintf('*Amplitude, name=Amp-%.0f, DEFINITION=TABULAR, time=TOTAL
TIME\n',i)
fprintf('0, 0, %f, 0, %f, 1, %f,
0\n',taminus(i),tavector(i),totaltime(i))
end

```

Code 9: modellMatrix.m

```

function modellnode = modellMatrix(nodeplace)

% modellMatrix.m is the node map profile for Model 1:
% H = 0.75" Sw = 1.0 "
% INPUTS:
% nodeplace, a place assigned by the loading program
% OUTPUTS:
% modellnode, the node number for assignment

```

```

A=[ 1;
    2;
    4;
    6;
    7;
    .
    . (file truncated)
    .
    66875;
    66876;
    66877];

modellnode=A(nodeplace);
end

```

Code 9: hephastus_94J_impulse

```

% hephaestus_94J_impulse.m creates diary files for the loading and
% time data for each of the seven models, F series, for conditions
% producing an equivalent impulse to Helmstetter's 94 J test.

```

```
warning off MATLAB:m_warning_end_without_block
```

```

A1 = 47.189026; %kg TNT
A2 = 47.0345194; %kg TNT
A3 = 46.738262; %kg TNT
A4 = 47.1112259; %kg TNT
B = 0.25; % m
C = 0; % ft above sea level

```

```

% MODEL 1F
diary model1F_loads_94J.txt
model1Floading(A1,B,C)
diary off
diary model1F_times_94J.txt
model1Ftimedata(A1,B,C)
diary off

```

```

% MODEL 2F
diary model2F_loads_94J.txt
model2Floading(A2,B,C)
diary off
diary model2F_times_94J.txt
model2Ftimedata(A2,B,C)
diary off

```

```

% MODEL 3F
diary model3F_loads_94J.txt
model3Floading(A2,B,C)
diary off

```

```

diary model3F_times_94J.txt
model3Ftimedata (A2,B,C)
diary off

% MODEL 4F
diary model4F_loads_94J.txt
model4Floading (A3,B,C)
diary off
diary model4F_times_94J.txt
model4Ftimedata (A3,B,C)
diary off

% MODEL 5F
diary model5F_loads_94J.txt
model5Floading (A4,B,C)
diary off
diary model5F_times_94J.txt
model5Ftimedata (A4,B,C)
diary off

% MODEL 6F
diary model6F_loads_94J.txt
model6Floading (A2,B,C)
diary off
diary model6F_times_94J.txt
model6Ftimedata (A2,B,C)
diary off

% MODEL 7F
diary model7F_loads_94J.txt
model7Floading (A2,B,C)
diary off
diary model7F_times_94J.txt
model7Ftimedata (A2,B,C)
diary off

```

Code 10: regressionFit.m

```

% regresstionFit.m fits a nonlinear least squares regression to the
% panel geometry (web spacing and height) based on maximum moment
% INPUTS: Sw (ins)
%         H (ins)
%         Mmax (kip-in)
% OUTPUTS: alpha (exponent on Sw)
%          beta (exponent on H)
%          K (constant)
%          Graph of moment as a surface in Sw and H

close all
clear all

```

```

% Web Spacings
Sw1 = 1;
Sw2 = 1.5;
Sw3 = 1.5;
Sw4 = 2;
Sw5 = 2;
Sw6 = 3;
Sw7 = 3;
Sw = [Sw1 Sw2 Sw3 Sw4 Sw5 Sw6 Sw7]';

% Stiffener Heights
H1 = 0.75;
H2 = 0.75;
H3 = 1;
H4 = 1;
H5 = 1.5;
H6 = 1.5;
H7 = 2;
H = [H1 H2 H3 H4 H5 H6 H7]';

% Maximum Moment from Probe
M1 = 397.2728107;
M2 = 149.9206643;
M3 = 289.7020811;
M4 = 115.580612;
M5 = 201.9273382;
M6 = 118.9713259;
M7 = 280.1077387;

Mmax = [M1; M2; M3; M4; M5; M6; M7];

LnSw = log(Sw);
LnH = log(H);
LnM = log(Mmax);
K = ones(7,1);

A = [LnSw LnH K];

C = (A'*A)\(A'*LnM);

disp('Values')
alpha1 = C(1)
beta = C(2)
K = exp(C(3))

for i=1:7
MTheoretical(i) = [Sw(i)^alpha1*H(i)^beta*K];
end

disp('Theoretical Moments:')
MTheoretical'

```

```

[SwAxis,HAxis]=meshgrid(1:0.01:3,0.75:0.01:2);

hold on
surf(SwAxis,HAxis,SwAxis.^alpha1.*HAxis.^beta.*K,'EdgeColor','none')
XLABEL('Stiffener Spacing')
YLABEL('Stiffener Height')
ZLABEL('Maximum Moment')
alpha(0.5)

for i = 1:7

plot3(Sw(i),H(i),Mmax(i),'marker','*','color','b','MarkerSize',10);
end
hold off

```

APPENDIX B: ERROR ANALYSIS

The table below is the statistical analysis performed on the theoretical and probed moments.

Theoretical	Measured	Summation, Theoretical	Summation, Measured	(ti-t)	(mi-m)	Summation, (mi-m)(ti-t)
360.5744	397.27281	20452.22784	30746.47542	143.01129	175.3467	25076.56118
144.9869	149.92066	5267.30688	5184.780116	-72.57621	-72.0054	5225.880593
255.5141	289.70208	1440.277317	4593.586118	37.950986	67.776	2572.165991
133.8706	115.58061	7004.436947	11309.3589	-83.69251	-106.345	8900.31973
297.5253	201.92734	6393.951144	399.9497371	79.962186	-19.9987	-1599.143233
119.6349	118.97133	9589.935153	10599.68172	-97.92821	-102.955	10082.17538
210.8356	280.10774	45.25944846	3385.105232	-6.727514	58.18166	-391.4179298
AVG: 217.563114	221.92608					
		VARIANCE:	7170.484962	9459.848176	σ_{MWMF} =	7123.791673
		STD.				
		DEVIATION:	84.67871611	97.26175084		
		R =	0.864957687			
		R²=	0.7481518			

APPENDIX C: FINITE ELEMENT CODES

FEM Code 1: Mode Shape File (model 1 shown)

```
*NODE, NSET=GLOBAL
  1, 18.2,-3.578268E-8, 1.0500002
  2, 18.15,-3.568245E-8, 1.0500002
  3, 0.8,-2.012776E-9, 0.15
.
.
.
102242, 18.15, 1.8999999, 0.9000004
102243, 18.15, 1.8999999, 0.9500004
102244, 18.15, 1.8999999, 1.0000005
*ELEMENT, TYPE=C3D8, ELSET=P2
  1, 247, 476, 477, 246, 495, 325, 485, 494
  2, 240, 469, 470, 239, 247, 476, 477, 246
  3, 233, 462, 463, 232, 240, 469, 470, 239
.
.
.
9646, 8579, 8792, 8785, 8572, 8927, 8727, 8726, 8563
9647, 8572, 8785, 8778, 8565, 8563, 8726, 8725, 8925
9648, 8565, 8778, 8723, 8510, 8925, 8725, 8905, 8922
*ELEMENT, TYPE=C3D8, ELSET=P1
27699, 17328, 17329, 9015, 8966, 19135, 18401, 28549, 26274
27700, 8966, 9015, 9016, 19132, 26274, 28549, 28550, 25918
27701, 19132, 9016, 9017, 8968, 25918, 28550, 28551, 25562
.
.
.
117146, 102242, 65040, 64684, 102243, 75187, 63609, 63608, 75186
117147, 102243, 64684, 64328, 102244, 75186, 63608, 75092, 75185
117148, 102244, 64328, 67304, 66856, 75185, 75092, 67305, 66857
*MPC
  PIN, 4543, 73466
  PIN, 4598, 56652
  PIN, 4597, 57008
```

```

.
.
.
  PIN,    58,   57189
  PIN,    59,   56833
  PIN,    10,   73285
*ELSET, ELSET=OUT_CONT, GENERATE
1,360,1
81449,117148,1
** Femap with NX Nastran Property 1 : Core
*ORIENTATION, NAME=S0, DEFINITION=COORDINATES,
SYSTEM=RECTANGULAR
  1.,    0.,    0.,    0.,    1.,    0.
*SOLID SECTION, ELSET=P1, MATERIAL=M1, ORIENTATION=S0
** Femap with NX Nastran Property 2 : Facesheets
*SOLID SECTION, ELSET=P2, MATERIAL=M2, ORIENTATION=S0
*MATERIAL, NAME=M1
*ELASTIC, TYPE=ISOTROPIC
  3440000.,  0.324,    0.
*DENSITY
  0.000112
*MATERIAL, NAME=M2
*ELASTIC, TYPE=ENGINEERING CONSTANTS
  3673806.,3673806.,1952208.,0.12,0.29,0.29,752746.,759998.
  759998.,0.
*DENSITY
  0.000175
*CONDUCTIVITY, TYPE=ORTHO
  0.
*BOUNDARY
  8966,  1
  8966,  2
  8966,  3
  8966,  4
  8966,  5
  8966,  6
.
.
.
28448,  1
28448,  2
28448,  3
28448,  4

```

```
28448, 5
28448, 6
** Load Step 1 -----
*STEP, INC=100
Untitled
*FREQUENCY, EIGENSOLVER=LANCZOS
  10, , , ,
*NODE PRINT, FREQUENCY=1
  U,
*FILE FORMAT, ASCII
*NODE FILE, FREQUENCY=1
  U,
*BOUNDARY, OP=NEW
8966, 1
8966, 2
8966, 3
8966, 4
8966, 5
8966, 6
.
.
.
28448, 1
28448, 2
28448, 3
28448, 4
28448, 5
28448, 6
*END STEP
```

FEM Code 2: ABAQUS Loaded Model (model 1 shown)

*NODE, NSET=GLOBAL

1, 18.2,-3.578268E-8, 1.0500002
2, 18.15,-3.568245E-8, 1.0500002
3, 0.8,-2.012776E-9, 0.15
4, 18.1,-3.558222E-8, 1.0500002
5, 0.8, -1.34185E-9, 0.35

.
.
.

102240, 18.15, 1.7999999, 1.0000005
102241, 18.15, 1.8999999, 0.8500003
102242, 18.15, 1.8999999, 0.9000004
102243, 18.15, 1.8999999, 0.9500004
102244, 18.15, 1.8999999, 1.0000005

*ELEMENT, TYPE=C3D8R, ELSET=P4

1, 247, 476, 477, 246, 495, 325, 485, 494
2, 240, 469, 470, 239, 247, 476, 477, 246
3, 233, 462, 463, 232, 240, 469, 470, 239
4, 226, 455, 456, 225, 233, 462, 463, 232
5, 212, 441, 442, 211, 219, 448, 449, 218

.
.
.

356, 8597, 8802, 8795, 8590, 8596, 8803, 8796, 8589
357, 8590, 8795, 8788, 8583, 8589, 8796, 8789, 8582
358, 8576, 8781, 8774, 8569, 8575, 8782, 8775, 8568
359, 8569, 8774, 8719, 8917, 8568, 8775, 8909, 8918
360, 8583, 8788, 8781, 8576, 8582, 8789, 8782, 8575

*ELEMENT, TYPE=C3D8R, ELSET=P2

824, 67596, 63241, 67508, 489, 67597, 63240, 67572, 39
825, 63241, 62885, 42, 67508, 63240, 62884, 67642, 67572
826, 62885, 62529, 67678, 42, 62884, 67615, 100, 67642
827, 62529, 67623, 67511, 67678, 67615, 67578, 67644, 100
828, 67623, 61817, 315, 67511, 67578, 67613, 102, 67644

.
.
.

9644, 8593, 8806, 8799, 8586, 8929, 70518, 8961, 8561
9645, 8586, 8799, 8792, 8579, 8561, 8961, 70520, 70551
9646, 8579, 8792, 8785, 8572, 70551, 70520, 8726, 70672
9647, 8572, 8785, 8778, 8565, 70672, 8726, 70522, 8925
9648, 8565, 8778, 8723, 8510, 8925, 70522, 70523, 70548

```

*ELEMENT, TYPE=C3D8R, ELSET=P1
27699, 17328, 17329, 9015, 8966, 19135, 18401, 28549, 26274
27700, 8966, 9015, 9016, 19132, 26274, 28549, 28550, 25918
27701, 19132, 9016, 9017, 8968, 25918, 28550, 28551, 25562
27702, 8968, 9017, 9018, 19130, 25562, 28551, 28552, 25206
27703, 19130, 9018, 9019, 8970, 25206, 28552, 28553, 24850
.
.
.
117144, 62893, 63612, 65396, 102241, 75087, 75088, 63610, 75188
117145, 102241, 65396, 65040, 102242, 75188, 63610, 63609, 75187
117146, 102242, 65040, 64684, 102243, 75187, 63609, 63608, 75186
117147, 102243, 64684, 64328, 102244, 75186, 63608, 75092, 75185
117148, 102244, 64328, 66676, 66228, 75185, 75092, 66677, 66229
*ELSET, ELSET=OUT_CONT, GENERATE
1,360,1
81449,101866,1
*SURFACE, NAME=SURF1, TYPE=ELEMENT
P1
P2
P4
*CONTACT
*CONTACT INCLUSIONS
SURF1
*Amplitude, name=Amp-1, DEFINITION=TABULAR, time=TOTAL TIME
0, 0, 0.000024, 0, 0.000025, 1, 0.034052, 0
*Amplitude, name=Amp-2, DEFINITION=TABULAR, time=TOTAL TIME
0, 0, 0.000024, 0, 0.000025, 1, 0.034307, 0
*Amplitude, name=Amp-3, DEFINITION=TABULAR, time=TOTAL TIME
0, 0, 0.000024, 0, 0.000025, 1, 0.034563, 0
.
.
.
*Amplitude, name=Amp-7516, DEFINITION=TABULAR, time=TOTAL TIME
0, 0, 0.000024, 0, 0.000025, 1, 0.034563, 0
*Amplitude, name=Amp-7517, DEFINITION=TABULAR, time=TOTAL TIME
0, 0, 0.000024, 0, 0.000025, 1, 0.034307, 0
*Amplitude, name=Amp-7518, DEFINITION=TABULAR, time=TOTAL TIME
0, 0, 0.000024, 0, 0.000025, 1, 0.034052, 0
*ORIENTATION, NAME=S0, DEFINITION=COORDINATES,
SYSTEM=RECTANGULAR
1., 0., 0., 0., 1., 0.
*SOLID SECTION, ELSET=P1, MATERIAL=M1, ORIENTATION=S0

```

```

*SOLID SECTION, ELSET=P2, MATERIAL=M2, ORIENTATION=S0
*SOLID SECTION, ELSET=P4, MATERIAL=M4, ORIENTATION=S0
** Femap with NX Nastran Material 4 : Brittle Cracking
*MATERIAL, NAME=M4
*ELASTIC, TYPE=ISOTROPIC
  1800000., 0.324, 0.
*BRITTLE CRACKING, TYPE=STRAIN
3600, 0,
1, 0.002,
*BRITTLE SHEAR, TYPE=RETENTION FACTOR
1, 0,
1, 0.002
*BRITTLE FAILURE, CRACKS=1
0.002,
*DENSITY
  0.000112
*MATERIAL, NAME=M1
*ELASTIC, TYPE=ENGINEERING CONSTANTS
3440000,3440000,1800000,0.324,0.28,0.28,800000,435000
435000,0.
*DENSITY
  0.000112
*MATERIAL, NAME=M2
*ELASTIC, TYPE=ENGINEERING CONSTANTS
3673806.,3673806.,1952208.,0.12,0.29,0.29,752746.,759998.
759998.,0.
*DENSITY
  0.000175
*CONDUCTIVITY, TYPE=ORTHO
  0., 0., 0., 0.
*BOUNDARY
8966, 1
8966, 2
8966, 3
8966, 4
8966, 5
8966, 6
.
.
.
28448, 1
28448, 2
28448, 3

```

```

28448, 4
28448, 5
28448, 6
** Load Step 1 -----
*IMPERFECTION, FILE=model1E_mode_shape, STEP=1
9, 0.03
*STEP
*Dynamic, Explicit, ELEMENT BY ELEMENT
, .02,,
*Bulk Viscosity
0.06, 1.2
*BOUNDARY, OP=NEW
8966, 1
8966, 2
8966, 3
8966, 4
8966, 5
8966, 6
.
.
.
28448, 1
28448, 2
28448, 3
28448, 4
28448, 5
28448, 6
*CLOAD, OP=NEW, amplitude=Amp-1
1, 2, -6.477557
*CLOAD, OP=NEW, amplitude=Amp-2
2, 2, -12.983632
*CLOAD, OP=NEW, amplitude=Amp-3
.
.
.
*CLOAD, OP=NEW, amplitude=Amp-7516
66875, 2, -13.012157
*CLOAD, OP=NEW, amplitude=Amp-7517
66876, 2, -12.983632
*CLOAD, OP=NEW, amplitude=Amp-7518
66877, 2, -6.477557
*OUTPUT, FIELD, NUMBER INTERVALS=200, VARIABLES=ALL
*END STEP

```